Utrecht University

Faculty of Science
Department of Physics and Astronomy

Galaxy speed control

Investigating intrinsic alignment of galaxies with the large scale velocity field

Bachelor Thesis
Institute for Theoretical Physics

Author:
Iris van Gemeren
Utrecht University

Supervisor:
Dr. N.E. Chisari
Utrecht University
10-06-2020

Abstract

In this thesis the intrinsic alignment effect of the correlation between shapes of galaxies and the velocity field on large scales is investigated. As it could be additional to the probes that exist to look at the large scale structure of the universe. The large scale structure can give valuable information about the formation and evolution of the universe which can help improve the cosmological model. The velocity-shape correlation is already investigated in simulations, giving promising results. The prediction done in this thesis is on the measurability of the correlation with the data from upcoming galaxy surveys such as the LSST survey. This prediction gave a fractional error for the alignment strength of 0.022 compared to 0.0011 for the already measured galaxy density-shape correlation. The signal to noise ratio for this correlation is 263 compared to 349. The same is done for the spectroscopic 4MOST survey to get around weak lensing contamination. The fractional error for the alignment strength is 0.11 for the velocity-shape correlation compared to 0.058 for the galaxy-shape correlation. The signal to noise ratio is for this survey respectively 55 and 101. This can be interpreted as promising for the measurability of velocity-shape correlation.

Also the improvement that this correlation could bring on three applications is discussed. From theoretical point of view it seems that adding velocity-shape correlation could improve on constraining observational selection effects that arise trying to extract cosmological information from the clustering of galaxies. A rough prediction on using multiple shape estimates to determine the scale dependence of the alignment model on small scales, points to an improvement after implementing this correlation. The effect of implementing velocity-shape correlation to better constrain primordial anisotropic non-Gaussianity after an estimate does not seem to give any enhancement. Although the comparison with existing results is not that straight forward to make.

Contents

1   Introduction

Our Universe is a mysterious place, it is also very big and has a long history. Cosmologists study the origin and evolution of our big universe and seek for the answers of the many open questions. Piece by piece, scientists try to build a picture of the structure and evolution of the universe. To get the information, one observes with large telescopes on earth and in space the radiation and recently also the gravitational waves that come from far away objects.

The structure of the universe can be described by looking at the distribution of stars. Large bound collections of stars result in galaxies, as the Sun in our galaxy, the Milky Way. Galaxies then form galaxy groups and those form galaxy clusters. The largest structures are walls and filaments separated by voids. These structures create a sponge like structure also called the cosmic web and the large scale structure. At the largest scales (> 100 Mpc)[1] the universe is approximately isotropic and homogeneous; the universe is the same in respectively all directions and all locations, this is known as the cosmological principle (Ryden, 2017, p.12).

To describe the structure and evolution of the universe, cosmological models are used. These models are mathematical descriptions of how the scaling of the universe changes in time, expressed in the different building blocks of our universe. The most common used model is the Lambda Cold Dark Matter (Lambda-CDM) model, it is the simplest and best model that corresponds with the observations for so far. The model is based on the cosmological principle and the expansion of spacetime and it assumes general relativity is an accurate description of gravity. It describes how our universe consists of radiation, baryonic matter, dark matter and dark energy. Cosmologists try with theories, simulations and observations to improve the model and determine, for example, how much of all the components really exists in the universe now and since formation. The real nature of dark matter and dark energy is still unknown. Scientists think dark matter should be there because gravity effects of objects in space are often much larger than should be relative to the observed matter, so there is much more 'unseen matter'. This was for example measured for the Bullet cluster in Clowe et al. (2006) which is a famous example of the evidence for dark matter. Our universe does not only expand, this expansion also accelerates. Therefore there should be a force that causes this acceleration; dark energy (first evidence came form supernovae measurements from Riess et al. 1998 and Perlmutter et al. 1999). Both looking at structure and acceleration of the universe can give more information about those mysterious forms of matter and energy. An elaborate overview of the most established methods for measurements on structures and acceleration of the universe is given by Weinberg et al. (2013), a couple are discussed in section 2.1.

Cosmologists search for ways to probe the universe in order to get more information. A very successful one is the Cosmic Microwave Background (CMB) which consists of long wavelength radiation which is a left over from the early times when the universe was just expanded enough that radiation could escape. Looking at very small anisotropies in this more or less perfect isotropic radiation gave a ton of information about the early universe, but also about evolution and structures due to the interactions of the radiation on its way to our telescopes (Ryden, 2017, Ch 8).

---

[1]Parsec, pc, is a common unit in astronomy and cosmology. It is based on the parallax method to determine distances to stars. It is defined as the distance at which 1 AU (Astronomical Unit = distance Earth-Sun) substends an angle of 1/3600 degree = 1 arcsecond. 1pc $\approx 3.086 \times 10^{16}$m

Another method is to look at the large scale structure of the universe. A lot of information is imprinted in how the galaxies and larger structures interact and cluster. A popular probe for this is weak lensing (Dodelson, 2003, Ch 9). Light of stars in the background is bend due to the gravitational potential of a 'lens' galaxy in the foreground. The observed background galaxies are therefore deformed. Weak lensing is a statistical method; averaging over a lot of galaxies is needed to extract the weak lensing signal. When averaging, one assumes the shapes and orientations of the galaxies to be random, so the deformation of the shape is only due to weak lensing. However this seems not to be the case, because of intrinsic alignment effects with the underlying fields.

Intrinsic alignments are the correlations between the shapes, orientations or positions of galaxies relative to the large scale structure (one of the first descriptions given in Catelan et al. 2001). The focus of this thesis will be on intrinsic alignments with the underlying density field and the velocity field of the large scale structure. The tidal field resulting from the underlying density field causes galaxies to deform leading to a correlation between the shapes of galaxies and higher density places due to the gravitational attraction.

Knowing about intrinsic alignment effects is important to be able to account for them in weak lensing measurements, but currently one also started looking at intrinsic alignment as a probe itself (see Chisari and Dvorkin 2013). So far, most of the research focused on alignment of the galaxies relative to the density field, but lately Okumura et al. (2019) stated that it would be interesting and useful to look at alignment relative tot the velocity field as well. If a galaxy is pointed to a higher density, for example another galaxy, due to its gravitational attraction there should also be a correlation between the direction of the velocity of the galaxy and the shape of the other galaxy. This correlation could give more information on top of the correlation between galaxy positions and galaxy shapes. In linear theory the velocity is proportional to the density with a factor depending on the distance, so it is expected that the velocity correlation is amplified on large scales compared to the density.

Okumura et al. (2019) and follow up papers Okumura and Taruya (2020), Okumura et al. (2020) describe intrinsic alignment relative to the velocity field and test the result in simulations. In this thesis the correlation of the shapes of galaxies with the velocity field is also the main subject, but here the question is: 'Is the correlation of the shapes of galaxies with the velocity field measurable with data from upcoming galaxy surveys and if so, how can the information of this correlation be useful'. The results from the simulations of the previously referred papers are very positive and agree on large scales with the models. This points in the direction of the measurability of the velocity-shape correlation in data from upcoming galaxy surveys. Quite higher uncertainties are expected then estimated from the simulations.

This thesis is organised as follows. In the upcoming section (2) some background about the large scale structure and cosmological models is given (2.1), followed by a description of the mathematical tools needed for the further analysis (2.2). Then a more detailed description of intrinsic alignment effects (2.3) and the correlation of the shape of galaxies with the velocity field (2.4) is given. Ending the section of the technical chapters with a description of how to reconstruct the velocity field (2.5) and a prediction of the measurability of the correlation between the galaxy shapes and the velocity field with a Fisher forecast (2.6). A discussion of possible applications for the correlation between the galaxy shapes and the velocity field

is given in (3). Ending this thesis with a conclusion and discussion of the results (4) and an outlook for further research on this topic (5). The Appendix (A) provides a description of the Python library that was used for doing the predictions and a short overview of the upcoming galaxy survey LSST.

2   Technical chapters

The following sections are the main part of this thesis. Beginning with background information on some important key features in cosmology, leading towards the subject of intrinsic alignment. Further a toolbox of cosmological quantities and functions is built up to be able to perform a prediction of the measurability of the correlation between the shapes of galaxies and the large scale velocity field in the end.

2.1   The Large scale structure and cosmological models

Before diving into intrinsic alignment effects, some background information is needed to understand where it came from and why this effect is interesting and useful. Up till early in the 1900s most scientists assumed that the universe was flat and static, it was infinite in space and time. Even Einstein altered his Theory of General Relativity so it would describe a static universe instead of a expanding or collapsing one. Not much later, the results of the measurements of Edwin Hubble changed this view. This section is largely based on Ryden (2017). 2.1.1 is related to chapter 2, 2.1.2 is based on chapter 7 and 11.5, 2.1.3 on chapter 4, 5 and 10, 2.1.4 on chapter 8 and 11.6.

2.1.1   The expansion of the universe

In 1929 Hubble had estimated distances of galaxies of which he also knew the redshift z. Redshift and blueshift are phenomena seen when looking at electromagnetic radiation due to the Doppler effect. When a star/galaxy moves away from us, the wavelength of its radiation will be observed slightly lengthened, if it moves towards us the radiation will be more packed together resulting in a smaller observed wavelength. This change in the wavelength is defined as the redshift:

$$z = \frac{\lambda_{obs} - \lambda_{em}}{\lambda_{em}} = \frac{v}{c} \tag{1}$$

The latter equality is the classical relation for the Doppler shift with v the velocity of the star or galaxy and c the speed of light. When looking at a radiation spectrum of a star or galaxy, black absorption lines are observed. At those wavelengths the radiation is absorbed by the atomic elements in the star or galaxy, for example by hydrogen. When looking at the spectra of distant galaxies, these absorption lines are shifted in comparison to the lines in the spectra that are seen on earth. By comparing these two spectra, the shift in wavelength can be determined and hence the redshift or blueshift of the galaxy . When combining the redshift and distance measurements, Edwin Hubble found a linear relation between the two in Hubble (1929). The larger the distance, the higher the redshift. So at a larger distance, galaxies move faster away from us. This is expressed in the simple relation $v = H_0 d$, the velocity of a galaxy is proportional to its distance multiplied with the Hubble constant H_0, with the best current estimate from the latest measurements of the Planck satellite; $H_0 = 67.4 \pm 0.5$ km s^{-1}Mpc^{-1}[2] (see Planck Collaboration et al. 2018). This relation can be explained by saying

---

[2]This is not the whole story, the value given here comes from the Planck telescope which measures the constant from early universe observations. When local universe measurements are used, a value of $H_0 = 73.5 \pm 1.4$km s^{-1}Mpc^{-1} is obtained. It is still an open question if this tension can be solved.

that the universe is expanding. When expanding, every galaxy is moving away from us and at a greater distance, there is more expansion in between us and the galaxy, hence moving away with a greater velocity. So apart from the velocities that galaxies may have on their own, called peculiar velocities, they also move due to the expansion of the universe.

This linear relation is useful. If the velocity is substituted for the velocity in the Doppler shift relation, one gets

$$z = \frac{H_0}{c}d \tag{2}$$

which relates the redshift to the distance. Note that this relation is only valid on small scales because this expression is the linear term of a Taylor expansion for the redshift. For larger scales more complicated relations from General Relativity are required. With the linear relation one can see that redshift is also an approximate distance measurement in cosmology. The larger the distance, the longer it takes for light to reach us. Redshift is therefore also a measurement of time. The greater the redshift, the further away the object is, the longer it took for the light to reach the earth hence observed as it was many years ago. Light can be observed up till the distance that light had the time to reach us in the span of the age of our universe.

The expansion of the universe also implies that there was a time where the whole universe was packed together in a state of very high density and temperature and even a stat before that in a so called singularity. Current knowledge cannot say anything before that time but the time when this 'packed together' universe started expanding is generally called the Big Bang. It is now estimated that this happened 13.8 billion years ago, the age of our universe, at that moment space and time merged. As the universe expanded, it cooled down, radiation and matter became less dense. The four fundamental forces (gravity, electromagnetic, strong and weak nuclear force) became separated and subatomic particles and atoms could form. Under influence of gravity more dense regions of particles packed together and eventually formed the structures of stars and galaxies we see today.

2.1.2 Dark matter and dark energy

The Lambda-CDM model is currently the most accepted an used cosmological model to describe the formation and evolution of the universe (Planck Collaboration et al. 2018). It takes into account the composition of the universe as we observe it. The energy contribution in the universe consists approximately of 4.5% ordinary matter, 27% dark matter and 68.5% dark energy (2.1.4). The evidence for dark matter comes from observations of galaxies. It can be calculated that the gravitational effects of the observed matter would not be enough to prevent galaxies from flying apart, being able to form or to perform their observed movement, hence they should contain a lot more matter that can not be seen. What dark matter exactly is, is still an open question. Dark matter does not interact with ordinary matter, only with gravity. Dark matter is separated in hot dark matter and cold dark matter by its velocity. The Lambda-CDM model supports cold dark matter. Hot dark matter would imply that first supercluster size structures were formed and from that the galaxies, but observations show that first galaxies form and that they pack together to form clusters and super clusters. This can be explained with cold dark matter.

The largest scales in the universe are influenced by dark energy. Measurements of supernovae done by Riess et al. (1998) and Perlmutter et al. (1999) showed that the expansion of the universe is accelerating. This acceleration could not be explained with the current model at that time unless an extra energy form was introduced. There are different forms proposed for dark energy, the Lambda-CDM model uses the cosmological constant Λ. Λ is the energy density of dark energy in the field equations of general relativity. According to Einstein's mass energy relation this dark energy exerts gravitational effects. The cosmological constant has a negative pressure and therefore accelerates the expansion of the universe. The precise nature of dark matter and dark energy is one of the big unanswered questions in cosmology (or physics in general).

2.1.3   Cosmological models

Cosmological models are based on the Friedmann equation. This equation is first derived by Alexander Friedmann in 1922 (Friedmann 1922) from the field equations of Einstein's theory of General Relativity. It describes the expansion of space expressed in the so called scale factor $a(t)$. The scale factor is a dimensionless parameter that relates the distance to a object in space at time t to the distance to the same object at time t_0. This distance is called the proper distance and it increases due to the expansion of the universe. In general, one takes t_0 as the current time and $a(t_0)$ equal to 1. At t_0 the proper distance is equal to the comoving distance χ^3, this distance is corrected for the expansion of the universe, so does not change in time. The scale factor tells you at a given time how much the universe is expanded, the rate of the expansion is given by the Hubble parameter

$$H(t) = \frac{\dot{a}(t)}{a(t)} \tag{3}$$

with $\dot{a}$ the time derivative of the scale factor. At $t = t_0$, $H(t_0) = H_0$, the expansion rate at current time is the same as the Hubble constant from the Hubble law.
In general form, the Friedmann equation can be written as:

$$H(t)^2 = \left(\frac{\dot{a}}{a}\right)^2 = \frac{8\pi G}{3c^2}\epsilon(t) - \frac{\kappa c^2}{R_0^2 a^2} \tag{4}$$

Where the expansion rate is expressed in the energy density of the universe ϵ, to which all the components in the universe contribute (ordinary matter, dark matter, radiation, the cosmological constant), the curvature of space κ and the curvature radius R_0. The energy density can be derived from the Friedmann equation for a spatially flat universe ($\kappa = 0$):

$$\epsilon_c(t) = \frac{3c^2}{8\pi G}H(t)^2 \tag{5}$$

This energy density is called the critical energy density, if the energy density in our universe is greater than the value of ϵ_c, the universe will be positively curved ($\kappa = +1$) and for a

---

[3]The comoving distance can be calculated with $\chi = \int_{t_e}^{t} c\frac{dt'}{a(t')}$ with t_e the time of emission of the photons from the object detected by the observer and t the current time.

smaller value the universe will be negatively curved ($\kappa = -1$). Because the Hubble constant is approximately known, the present day critical density can be calculated $\epsilon_{c,0}(t) = 4870 \pm 290 \, \text{MeVm}^{-3}$. In the more intuitive mass density this would be $\rho_{c,0} = \frac{\epsilon_{c,0}}{c^2} = (8.7 \pm 0.5) \times 10^{-27} \, \text{kgm}^{-3}$ which is very small, about one proton per 200 liters. Even the hottest regions in space contain a few protons per liter. However the universe contains a lot of enormous voids with very low density. So on average, as it turns out, the density of our universe is very close to the critical density, meaning our universe is practically flat.

Often in cosmology the energy density is expressed in the dimensionless density parameter,

$$\Omega(t) = \frac{\epsilon(t)}{\epsilon_c(t)} \tag{6}$$

so for $\Omega = 1$ the universe is flat and for $\Omega < 1/ > 1$ the universe is respectively negatively or positively curved. The Friedmann equation can be expressed in this density parameter in the following way:

$$H(t)^2 = \frac{8\pi G}{3c^2}\epsilon(t) - \frac{\kappa c^2}{R_0^2 a^2} \tag{7}$$

$$H(t)^2 = \frac{8\pi G}{3c^2}\frac{\epsilon(t)}{\epsilon_c(t)}\frac{3c^2 H(t)^2}{8\pi G} - \frac{\kappa c^2}{R_0^2 a^2} \tag{8}$$

$$(1 - \Omega(t)) = -\frac{\kappa c^2}{R_0^2 a(t)^2 H(t)^2} \tag{9}$$

When the universe expands in time the right hand side of this equation does not change sign due to the squares, so the sign of Ω will not change in time. This means that if at present time a flat universe is measured, this would have been the case throughout the evolution of the universe.

With the present day version of the formula from above, the relation between the density, curvature and the Hubble constant is described.

$$(1 - \Omega_0) = -\frac{\kappa c^2}{R_0^2 H_0^2} \tag{10}$$

This can be used to substitute $\frac{\kappa}{R_0^2}$ in the Friedmann equation.

$$H(t)^2 = \frac{8\pi G}{3c^2}\epsilon(t) - \frac{H_0^2}{a(t)^2}(\Omega_0 - 1) \tag{11}$$

Dividing by H_0^2 gives:

$$\frac{H(t)^2}{H_0^2} = \frac{\epsilon(t)}{\epsilon_{c,0}} + \frac{1 - \Omega_0}{a(t)^2} \tag{12}$$

The advantage of writing the Friedmann equation like this, is that it now can be expressed in the different components of our universe. $\epsilon(t)$ is the energy density contributed by all the components, so can be written out as a sum of ϵ_x with x the component: matter(m), radiation(r) or cosmological constant(Λ). The different energy densities of the different species scale with different powers of the scale factor: $\epsilon_m(t) = \frac{\epsilon_{m,0}}{a^3}$, $\epsilon_r(t) = \frac{\epsilon_{r,0}}{a^4}$ and $\epsilon_\Lambda(t) = \epsilon_{\Lambda,0}$.

Implementing this in the Friedmann equation and writing the energy densities divided by the critical density as the density parameter, gives:

$$\frac{H(t)^2}{H_0^2} = \frac{\Omega_{r,0}}{a^4} + \frac{\Omega_{m,0}}{a^3} + \Omega_{\Lambda,0} + \frac{1 - \Omega_0}{a^2} \tag{13}$$

This is the general Benchmark Model for cosmology. Specific models specify which energy densities are present in the universe and what their values are. Also for other models in which dark energy is not described by the cosmological constant, the scaling of this energy density will not be constant in time. For the Lambda-CDM model, a flat universe is adopted, so the last term in (13) is zero and the dark energy is described by the cosmological constant as above. In cosmology, one tries to measure and constrain these parameters with data from the telescopes to check this Lambda-CDM model. Lamda-CDM describes the universe and its evolution pretty well, but it is not perfect, therefore there are also many versions of the extended Lambda-CDM model. For example, cosmological inflation can be added and it is not certain if the dark energy contribution is really constant in time, so there is also a model in which the dark energy contribution varies. The better the model, the better one can answer the big open questions about the universe, for example what the nature of dark matter and dark energy is.

An early period of accelerated expansion, called inflation, could solve particular problems that the Lambda-CDM model can not explain. These problems can be summarised in the following questions: Why the universe is homogeneous and isotropic, why the universe is nearly perfectly flat and why there are no magnetic monopoles, which in theory should be produced in the very hot early universe. Inflation is an epoch in the early universe when space was expanding exponentially. After this epoch the acceleration of the expansion slowed down. Cosmic inflation was first theorised by theoretical physicist Alan Guth in 1981 (Guth 1981). There are different inflation theories that try to describe the mechanism behind it, but there is no consensus yet. Current research tries to determine the best model. One way to do this is by measuring non-Gaussianity in the primordial tidal field (3.3). Inflation should have started from around 10^{-36} seconds after the Big Bang till 10^{-33}-10^{-32} seconds after. Due to the great expansion of space, quantum fluctuations are magnified and become the start of further structure growth. Simply said it can solve the problems stated above in the following way; the rapid expansion of space flattened out fluctuations, distributed monopoles immensely far apart and the distances that could not be causally connected to form a thermal equilibrium of matter and radiation were before the epoch small enough to reach equilibrium which leads to a homogeneous and isotropic distribution.

2.1.4 Probes of the large scale structure

To measure the parameters to determine the model that describes the universe best, one has a whole arsenal of methods, a few are mentioned here. One example is measuring type Ia supernovae. These supernovae act like standard candles for the distance in the universe. Because these supernovae have common properties in, among other things their exploding mechanism, which makes them standardizable. Distance measurements give information about the expansion of the universe and these measurements showed that the universe is accelerating. Because the acceleration of the universe is partly powered by dark energy, measuring the acceleration gives us more information about the nature of dark energy.

Another very successful probe is the cosmic microwave background (CMB). This is faint electromagnetic radiation, strongest in the microwave region of the radio spectrum, equally distributed in space. This radiation is originating from the early universe. After the big bang the universe was very dense and consisted of a cloud of freely moving protons and electrons, photons scattered of the electrons and could not escape. When the universe expanded, it cooled down and the protons and electrons formed neutral hydrogen atoms, this was the epoch of recombination. The photons could now escape and moved freely through space, this is called photon decoupling. These are the CMB photons that are now measured, but with much less energy because their wavelength is lengthened by the expansion of space. The CMB gives us a picture of the time of decoupling of the photons, also called the time of last scattering. The CMB radiation looks very homogeneous, it has a temperature of T = 2.725K from everywhere, but when looking in more detail, anisotropy is observed and this gives a lot of information. There are two kinds of anisotropy observed; primary anisotropy which is due to the effects that occurred around the time of last scattering and secondary anisotropy coming from the effects along the way to the observer, such as interactions with gas or gravitational potentials. The primary anisotropies give information about the curvature of the universe, how the number of baryons reduced in the early universe and the dark matter density in that time. Secondary anisotropies give information about the change of content in the universe in time and specific information about objects in the universe due to interaction with the CMB photons. An example is the kinetic Sunyaev Zeldovich effect which can be measured as a Doppler shift of the CMB photons due to scattering with the electrons in moving galaxies. This can be used to reconstruct the peculiar velocities of those galaxies (2.5).

When looking at the large structure of the universe and the clustering of galaxies a lot of information can be gathered from remains of processes during the formation and evolution of the universe. An example of such remains are Baryon Acoustic Oscillations (BAOs). In the very early times the universe was hot and packed together. Electrons, baryons and photons moved freely and formed a fluid. Two counteracting forces were active in this fluid, the overdense regions exerted gravitational attraction and the radiation and matter created a pressure outwards. This fluid of baryons and photons got compressed when near a overdense region, which increased the pressure, which leads to expanding of the fluid, this decreased the pressure and the fluid would be compressed again. In this way, waves got created called acoustic oscillations. Spherical waves consisting of baryons and photons moved outwards. When the universe expanded it cooled down and photons were no longer coupled to the matter and could escape. The higher dense regions of baryons of the waves remained, called the Baryon Acoustic Oscillations. These 'rings' together with the overdensity regions that contain dark matter, created anisotropies in the density field of the universe which attracted matter. This eventually grew to the structures of galaxies we see now. The BAOs are imprinted in the large structure, a higher population of galaxies is seen on the scales of this Baryon Acoustic Oscillation 'rings'. BAOs are used as a standard ruler, because their length is the distance that the waves could have travelled in the fluid before it cooled down, which stopped the propagating of the waves. When comparing the scale of BAOs today in the large scale to the one from predictions and for example from the CMB, one gets information about the expansion and acceleration of the universe, hence about the nature of dark matter.

The probe that is current of high interest and the focus point of galaxy surveys in present and near future is weak lensing. In the presence of a mass, the path of light is bent due to the gravitational potential of this mass. In rare occasions this deforms the image of distant galaxies in a way that an arc or multiple images of the galaxy is observed. This is called strong lensing. Most of the time the picture of distant galaxies is just a bit smeared out by the deflection of light on its way to the observer. It is not possible to detect this for a single galaxy or other sources in the background, but it is still possible to detect the foreground 'lensing' mass because of how the background sources systematically align around the lensing mass. This is called weak gravitational lensing, which is a statistical measurement, but can measure masses of objects without knowing the details of their composition. By comparing the statistical correlation functions that can be calculated with the cosmological model and the ones calculated with weak lensing the cosmological model can be checked and cosmological parameters constrained.

Weak lensing is a very powerful probe but there are many challenges. The smearing out of the background sources is very faint and averaging over many background sources is needed, the survey should therefore be very deep and wide, plus the image quality must good. Furthermore, the shape of the background galaxies must be calculated to measure the weak lensing effect. The problem is that galaxies are not circular, the measured ellipticity is a combination of the shape of the galaxies itself and the ellipticity due to the weak lensing effect. Therefore the measurement of background galaxies must be combined to average out the shape of the galaxy itself (this contaminant is called shape noise). Furthermore the orientation of this intrinsic ellipticities of the galaxies must be random so the alignments can be related to weak lensing.

This last assumption turned out not to be the case, the intrinsic ellipticities of galaxies are not entirely random due intrinsic alignments of galaxies and clusters. Intrinsic alignments are correlations of galaxy orientations or shapes with the surrounding fields, for example the mass overdensity field[4]. These alignments arise during formation and evolution of the galaxies. Examples are the stretching of galaxy shapes by the tidal field created by the mass distribution of the large scale structure, influence of the tidal torque on the angular momentum of a galaxy or movement along specific directions. Catelan et al. (2001) was one of the first to describe a model for the alignment of galaxies with the tidal field, called the linear alignment model (LA model). It is based on the tidal field created by the mass distribution in space which leads to a tendency of ellipticities of galaxies to point at higher density regions due to the gravitational attraction. From observations (Brown et al. 2002, Mandelbaum et al. 2006, Joachimi et al. 2011, Singh et al. 2015, Johnston et al. 2019, Samuroff et al. 2019) followed that Luminous Red Galaxies, which are generally elliptical type galaxies, follow the LA model well at large scales ($> 10h^{-1}\mathrm{Mpc}$)[5], on smaller scale a non-linear model (Hirata et al. 2007, Bridle and King 2007) is needed. For blue galaxies this alignment following the LA-model is not found yet (Mandelbaum et al. 2011).

---

[4]overdensity is the measure of how much the density at a certain position is above or below the average density

[5]h is called the reduced Hubble constant it is a way to express the Hubble parameter in, $h = H_0/(100\mathrm{km\,s}^{-1}\mathrm{Mpc}^{-1})$. This can be useful if one does not want to quantify the value of the Hubble constant, about which consists tension of what the real value would be. Therefore often in cosmology, parameters are expressed in terms of this reduced Hubble constant, so the parameter is independent of the value of h.

Investigating intrinsic alignment effects is important to improve on the weak lensing results, such as constraining cosmological parameters, but it is also a good probe on its own (see Chisari and Dvorkin 2013). For example when studying the correlation functions that come from describing the alignment signals, Baryon Acoustic Oscillations and non-Gaussianity in the primordial density field (3.3) can be seen.

For further calculations in this thesis the values for the cosmological parameters are coming from the latest measurements from the Planck satellite Planck Collaboration et al. (2018): $\Omega_{CDM} = 0.27$, $\Omega_b = 0.045$, $\Omega_\kappa = 0$, $h = 0.67$, $A_s = 2.1 \times 10^{-9}$, $n_s = 0.96$. Hereby does CDM stand for cold dark matter, b for baryons and is the matter density parameter defined as $\Omega_m = \Omega_{CDM} + \Omega_b$. A_s, n_s are the amplitude and the power of the primordial power spectrum respectively. The used distance unit is Mpc and the speed of light, c will be set to 1.

2.2   Correlation functions and power spectra

To describe intrinsic alignment effects of galaxies a few mathematical tools are needed. This description below will be largely based on chapter 7 and 9 of Dodelson (2003).
When trying to measure intrinsic alignment effects (IA effects) one needs to look at many galaxies and see if there is some correlation between the position, shape or orientation of the galaxies and the large scale structure. For doing this it is useful to work with a correlation function. On these large scales the growth of structure is determined by the attraction of gravity and the expansion of space by dark energy, causing the growth to be linear. On smaller scales gravity becomes more dominant and a more non-linear theory is needed, which can be calculated with simulations and higher order statistics. For the larger scales the correlation function encodes most of the information and higher order statistics are not needed. The correlation function calculates the statistical correlation between variables. One can have a auto-correlation function, when the two variables represent the same quantity and a cross-correlation function when two different variables are used. To be more concrete, in cosmology one refers to the correlation function as a two point auto-correlation function with the distance as variable. Two point means that two variables are taken into account. This correlation function gives the probability of finding two certain matter density levels separated at a certain distance. So if the correlation function gives a high value for a certain distance it means that there is a high probability of finding the same matter density at this distance. The galaxy density can be derived from the matter density via a bias (2.3.2). The correlation function of this galaxy density gives the probability of finding an other galaxy at a certain distance. The universe is more clustered at this distance, so galaxy density correlation gives a way to measure the clustering of galaxies at different scales.
The correlation function of (dark)[6] matter density can be calculated with:

$$\xi\left(\left|\mathbf{x}_1 - \mathbf{x}_2\right|\right) = \langle \delta\left(\mathbf{x}_1\right) \delta\left(\mathbf{x}_2\right)\rangle \tag{14}$$

where the angle brackets denote an averaging over all realizations of $\delta(\mathbf{x})$ and $\delta(\mathbf{x}) = (\rho(\mathbf{x}) - \bar{\rho})/\bar{\rho}$ is the overdensity, a dimensionless measure of the density at every position relative to the mean density $\bar{\rho}$. When writing the difference vector as: $r = \mathbf{x}_1 - \mathbf{x}_2$ one can write the correlation function as the integral:

$$\xi(r) = \frac{1}{V} \int d^3x \langle \delta(\mathbf{x}) \delta(\mathbf{x} + \mathbf{r})\rangle \tag{15}$$

For calculating cross-correlation functions the same formalism is used but instead of two $\delta(\mathbf{x})$, two different variables are taken.
The correlation function is related to the power spectrum $P(k)$ via a Fourier transform[7],

---

[6]Dark matter and matter are often used interchangeably because dark matter makes up the vast majority of all the matter in the universe

[7]The Fourier convention used in this thesis is

$$f(\vec{x}) = \int \frac{d^3k}{(2\pi)^3} e^{i\vec{k}\cdot\vec{x}} \tilde{f}(\vec{k})$$
$$\tilde{f}(\vec{k}) = \int d^3x e^{-i\vec{k}\cdot\vec{x}} f(\vec{x})$$

where k is the wavenumber defined as $k = \frac{2\pi}{\lambda}$ with dimension $\frac{1}{L}$

this power spectrum is actually the matter power spectrum because it is related to the auto-correlation function of the overdensity, but this matter power spectrum is often called the power spectrum. It is also often written as $P_{\delta\delta}(k)$ or $P_{lin}(k)$. The power spectrum includes the same information as the correlation function but in Fourier space which is often more convenient to work with. This power spectrum is related to the correlation function as follows:

$$\xi\left(|\mathbf{x}_1 - \mathbf{x}_2|\right) = \langle \delta\left(\mathbf{x}_1\right)\delta\left(\mathbf{x}_2\right)\rangle = \int \frac{d^3\mathbf{k}}{(2\pi)^3} P(k) e^{i\mathbf{k}(\mathbf{x}_1 - \mathbf{x}_2)} \tag{16}$$

To get the power spectrum from this definition one could use that $\int \frac{d^3\mathbf{k}}{(2\pi)^3} e^{i\mathbf{k}(\mathbf{x}_1 - \mathbf{x}_2)}$ is the Fourier transform of the three dimensional Dirac delta function. So if $\delta(\mathbf{k})$ is the Fourier transform of the overdensity then the power spectrum is given by:

$$\langle \delta(\mathbf{k})\delta\left(\mathbf{k}'\right)\rangle = (2\pi)^3 P(k)\delta^3\left(\mathbf{k} - \mathbf{k}'\right) \tag{17}$$

with δ^3 the three dimensional Dirac delta.
The matter correlation function gives the probability to have the same overdensity at a distance r from a random overdensity. The matter power spectrum breaks this probability up into the probability at characteristic lengths k, also called k-mode, which is proportional to 1/length. The matter power spectrum gives the measure for how much a certain k contributes to the total probability.

2.3   Intrinsic alignment statistics

Intrinsic alignment of galaxies is the collective term for the correlations between the positions, orientations and shapes of galaxies that originate during their formation and evolution with the underlying fields that trace the large scale structure of the universe. In this thesis the intrinsic alignment effect of stretching a galaxy shape due to the tidal field of the large scale structure is analysed. For studying this stretching, a way to describe the shape of a galaxy is needed. Therefore the ellipticity and the shear of a galaxy are defined. With the linear tidal alignment model (LA model) it can be described how this intrinsic ellipticity of a galaxy can be related to the tidal field on large scales. This section relies on the descriptions of the linear alignment model in Catelan et al. (2001), Chisari and Dvorkin (2013), Singh et al. (2015), Blazek et al. (2011), Kurita et al. (2020) and Okumura et al. (2019).

2.3.1   Galaxy shapes

The ellipticity of a galaxy is defined in terms of the ratio (q) between the minor and major axis of the best fit ellipse of the galaxy image:

$$e = \left(1 - q^2\right) / \left(1 + q^2\right) \tag{18}$$

For convenience this can be decomposed in the following components:

$$e_{(+,x)} = e[\cos(2\theta), \sin(2\theta)] \tag{19}$$

With θ the angle between the x-axis and the position of the galaxy, see figure 3. The plus component describes the alignment in the radial direction or tangential direction relative to another galaxy if this term is respectively negative or positive. The cross term describes the alignment in the directions rotated 45 degrees relative to e_+, see figure 1.
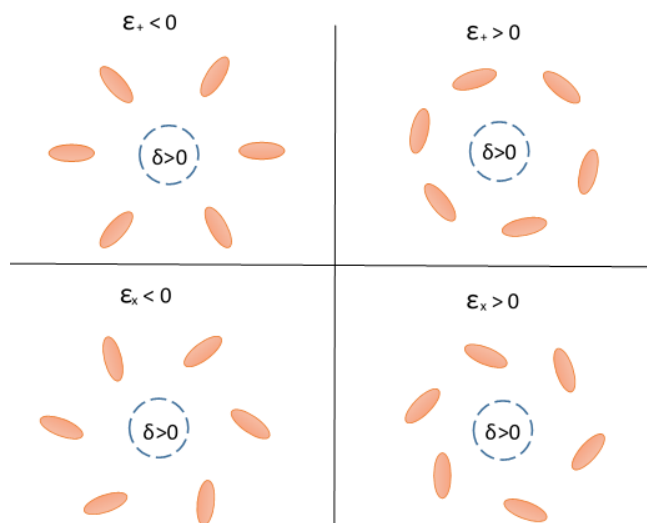

Figure 1: Schematic picture. The kinds of alignment the ellipticities of galaxies (red oval shapes) with a higher density region for the separate components of the ellipticity definition.

The change in this ellipticity is called the shear, γ, and can be expressed as $\gamma = e/2\mathcal{R}$ with $\mathcal{R}$ the factor that describes the response of the ellipticity to a distortion, for example the weak distortion by gravitational lensing. The shape of galaxies is measured as a projection on a 2D-plane perpendicular to the line of sight. The assumption is that the space is flat instead of curved, which is plausible, because the shape of galaxies is much smaller than the (local) curvature in space.
When the shape of a galaxy is observed, it consists of different contributions; a contribution of the intrinsic alignment effect due to the tidal field γ^I, a part is the effect of weak lensing γ^G and the random galaxy shapes which are independent of the other effects γ^{random}.

$$\gamma^{observed} = \gamma^{random} + \gamma^G + \gamma^I \tag{20}$$

To study intrinsic alignment of galaxies the γ^I term is of interest. From now on, when the shape/shear is defined, γ^I is meant, so the superscript I will be omitted.

2.3.2   The linear alignment model

The linear (tidal) alignment model is one of the simplest models to describe the correlation between γ^I and the tidal field (see Catelan et al. 2001). This model is based on the following reasoning; when a overdensity region collapses due to gravitational attraction and forms a galaxy, this galaxy undergoes the effect from the tidal gravitational field. A constant tidal gravitational field describes the change in gravitational acceleration for every point in space. A galaxy during formation in such a field will feel a different gravitational acceleration on one side then on the other. The gravitational collapse of the galaxy is then not spherically symmetric but exerts some anisotropy. This effect is sketched in figure 2. Galaxies should retain some left over of this effect during formation. Especially elliptical galaxies, which rotate less, are more likely to line up with the tidal field.

Figure 2: Based on figure 1 of Catelan et al. (2001). Schematic picture of how a constant tidal field can influence the shape. The arrows show the strength and direction of the gravitational field. The left picture describes alignment of the galaxy with the stretching axis of the tidal field and the right picture describes alignment of the galaxy with the compressing axis of the tidal field.

According to the linear alignment model (LA model) the shape of galaxies can be combined with the tidal field with the following linear function:

$$\gamma_{(+,\times)}(\mathbf{x}) = -\frac{C_1}{4\pi G} \left(\nabla_x^2 - \nabla_y^2, 2\nabla_x \nabla_y \right) S\left[\Psi_P(\mathbf{x}) \right] \tag{21}$$

The shape γ is related to the potential of the primordial universe Ψ_P, the quadratic terms of the potential are needed to describe the change in shape. In Catelan et al. (2001) this is explained as follows; when the potential is Taylor expanded around the origin, the zeroth order term has no effect. The linear term leads to a translation, because this describes a constant gravitational field. Yet the quadratic term gives a change of the shape. This is because the quadratic term describes the changes in the gravitational field, hence the tidal field. C_1 is a normalization parameter that describes the strength of the alignment. It is defined that a positive C_1 corresponds to a galaxy alignment along the stretching axis of the tidal field and a negative C_1 alignment along the compressing axis of the tidal field, see figure 2. Galaxies tend to align with the stretching axis of the tidal field (Catelan et al. 2001), so a positive C_1. This results in a negative γ, alignment configurations will therefore look like the top left side of figure 1 (the configurations for cross ellipticity on the bottom of figure 1 are not physical as will be shown below (2.3.2)).

S is a smoothing filter that evens out fluctuations. This factor is often neglected because it has no significant effects on large scales ($> 10h^{-1}\mathrm{Mpc}$) were this model is applicable. G is the gravitational constant.

The primordial potential is calculated at the redshift of primordial times, this is just an assumption. But as shown in Singh et al. (2015), Okumura et al. (2019) and Chisari and Dvorkin (2013) this is validated because the observations of alignments of Luminous Red Galaxies follow the linear alignment model based on this redshift at primordial times.

On large scales in the linear regime, the density field is linear and is related to the gravitational potential via the Poisson equation. In Fourier space this gives:

$$\Psi_P(\mathbf{k}) = -4\pi G \frac{\bar{\rho}(z)}{D(z)} a^3 k^{-2} \delta(\mathbf{k}) \tag{22}$$

Here is $\bar{\rho}(z)$ the average density in the universe, $\delta(\mathbf{k})$ the dark matter overdensity and D(z) the growth function which describes the growth of the matter perturbations at late times; overdense regions attract more matter and becoming more overdense. This potential in Fourier space can be substituted in the Fourier transform of (21) which would be[8]:

$$\gamma_{(+,\times)}(\mathbf{k}) = \frac{C_1}{4\pi G}(k_x^2 - k_y^2, 2k_x k_y)\Psi_P(\mathbf{k}) \tag{23}$$

However when shapes are observed, only the density weighted intrinsic ellipticity can be measured, because only at the positions of galaxies, the shape of a galaxy can be measured. The density weighted ellipticity is given by $\tilde{\gamma} = (1 + \delta_g)\gamma$. δ_g is the galaxy overdensity and it is related to the dark matter overdensity via the galaxy linear bias term b_g, $\delta_g = b_g \delta$. Only dark matter densities can be measured at positions of galaxies, but it is not a 1-1 relation, there can be dark matter overdensities where there is no galaxy. Often the extra terms due to the weighting of the shape can be neglected when calculating the correlation function due to higher orders of the density field. However this density weighted shape expression is discussed here because it is in some cases not negligible (see 3.1). The Fourier transform of the density weighted ellipticity will then be:

$$\tilde{\gamma}_{(+,\times)}(\mathbf{k}) = (1 - b_g\delta)\frac{C_1}{4\pi G}(k_x^2 - k_y^2, 2k_x k_y)\Psi_P(\mathbf{k}) \tag{24}$$

---

[8]To see this, the Fourier transform of the nabla operator is $-i\mathbf{k}$

The overdensity term in the potential will be multiplied with the overdensity from the weighting term. A product of density fields becomes a convolution when they are Fourier transformed[9].

$$\tilde{\gamma}_{(+,\times)}(\mathbf{k}) = -\frac{C_1 a^3 \bar{\rho}(z)}{D(z)} \int d^3\mathbf{k_1} \frac{(k_{2x}^2 - k_{2y}^2, 2k_{2x}k_{2y})}{k_2^2} \delta(\mathbf{k_2})(\delta^{(3)}(\mathbf{k_1}) + \frac{b_g}{(2\pi)^3}\delta(\mathbf{k_1})) \qquad (25)$$

$$\tilde{\gamma}_{(+,\times)}(\mathbf{k}) = -\frac{C_1 a^3 \bar{\rho}(z)}{D(z)} \left[\frac{(k_x^2 - k_y^2, 2k_xk_y)}{k^2}\delta(\mathbf{k}) + \int \frac{d^3\mathbf{k_1}}{(2\pi)^3} \frac{(k_{2x}^2 - k_{2y}^2, 2k_{2x}k_{2y})}{k_2^2} b_g \delta(\mathbf{k_2})\delta(\mathbf{k_1}) \right] \qquad (26)$$

$\delta^{(3)}$ describes the three dimensional Dirac delta and $\mathbf{k_2} = \mathbf{k} - \mathbf{k_1}$. This is the expression of the shape of a galaxy according the LA model. It can be used to calculate correlation functions and power spectra to be able to compare the model to measurements and simulations.

In this thesis the cross-correlations between the galaxy density and the shape and the velocity field and the shape are of most interest. The cross-correlation between the galaxy density and the shape can be calculated as follows:

$$\xi_{gi} = \langle \delta_g(\mathbf{x})\tilde{\gamma}_i(\mathbf{x} + \mathbf{r}) \rangle \qquad (27)$$

with $i = (+, \times)$. When calculating $\xi_{g\times}$ this turns out to be zero. One can explain this by looking at the $\times$ component of the shape (see figure 1). When this is not zero, there would be a preferential rotational direction in the universe, which drives into the anisotropy argument of the universe at large scales. So to get the galaxy density-shape correlation, ξ_{g+} is calculated. Without loss of generality, the position $\mathbf{x}$ can be placed in the origin of the coordinate system, see figure 3.

$$\xi_{g+} = \langle \delta_g(\mathbf{0})\tilde{\gamma}_+(\mathbf{r}) \rangle \qquad (28)$$

---

[9]definition convolution

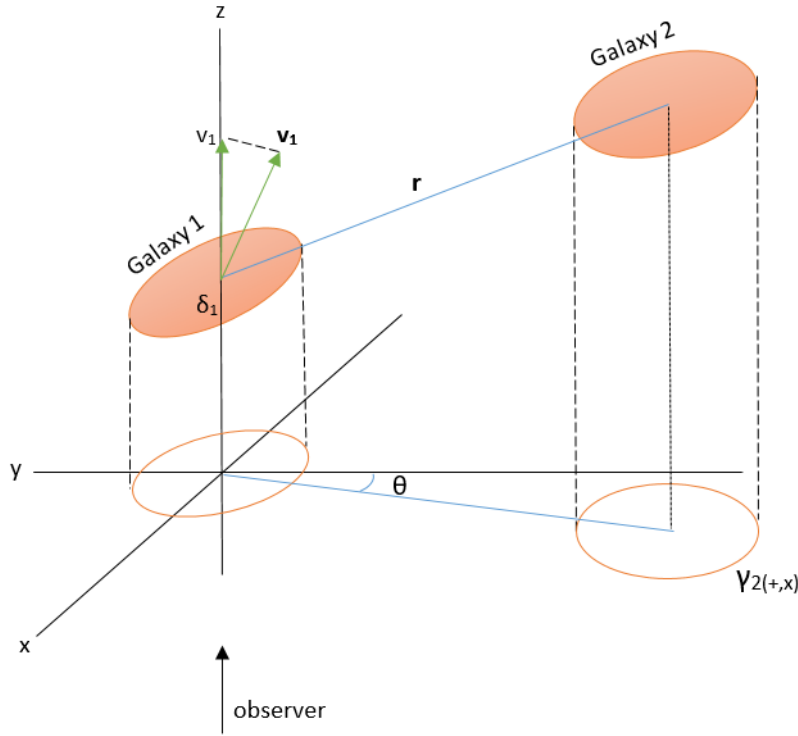$$(f * g)(t) \triangleq \int_{-\infty}^{\infty} f(\tau)g(t - \tau)d\tau$$

Figure 3: Schematic picture based on figure 1 of Okumura et al. (2019). When correlating galaxies a quantity of galaxy 1, for example δ, is correlated with another quantity, for example γ_+ of galaxy 2 at separation $\mathbf{r}$. This is done for a range of different r and for many different galaxy 1's. Angle θ and velocity vector $\mathbf{v}$ and component v are drawn for clarity of the used quantities.

Then the reversed Fourier transform of $\tilde{\gamma}_+$ and δ_g are needed.

$$\tilde{\gamma}_+(\mathbf{r}) = \int \frac{d^3\mathbf{k}}{(2\pi)^3} e^{i\mathbf{k}\mathbf{r}} \tilde{\gamma}_+(\mathbf{k}) \tag{29}$$

$$\delta_g(0) = b_g\delta(0) = b_g \int \frac{d^3\mathbf{k}}{(2\pi)^3} \delta(\mathbf{k}) \tag{30}$$

Now the correlation function can be calculated. Only the terms up to quadratic order in δ are taken into account. This means that the second term of (26) will be neglected because it becomes third order after correlating it with the galaxy density.

$$\xi_{g+} = \left\langle b_g \int \frac{d^3\mathbf{k}'}{(2\pi)^3} \delta(\mathbf{k}') \times (-1) \frac{C_1 a^3 \bar{\rho}(z)}{D(z)} \int \frac{d^3\mathbf{k}}{(2\pi)^3} e^{i\mathbf{k}\mathbf{r}} \frac{(k_x^2 - k_y^2)}{k^2} \delta(\mathbf{k}) \right\rangle \tag{31}$$

$$\xi_{g+} = -\frac{C_1 b_g a^3 \bar{\rho}(z)}{D(z)} \int \frac{d^3\mathbf{k}'}{(2\pi)^3} \int \frac{d^3\mathbf{k}}{(2\pi)^3} e^{i\mathbf{k}\mathbf{r}} \frac{(k_x^2 - k_y^2)}{k^2} \langle \delta(\mathbf{k}')\delta(\mathbf{k}) \rangle \tag{32}$$

Now (17) can be used to substitute the average over the densities. This also removes one integral over k because of the Dirac delta which appears after substitution.

$$\xi_{g+} = -\frac{C_1 b_g a^3 \bar{\rho}(z)}{D(z)} \int \frac{d^3 \mathbf{k}'}{(2\pi)^3} \int \frac{d^3 \mathbf{k}}{(2\pi)^3} e^{i\mathbf{kr}} \frac{(k_x^2 - k_y^2)}{k^2} (2\pi)^3 P(k) \delta^3(\mathbf{k} - \mathbf{k}') \tag{33}$$

$$\xi_{g+} = -\frac{C_1 b_g a^3 \bar{\rho}(z)}{D(z)} \int \frac{d^3 \mathbf{k}}{(2\pi)^3} e^{i\mathbf{kr}} \frac{(k_x^2 - k_y^2)}{k^2} P(k) \tag{34}$$

Then a switch to cylindrical coordinates is made:

$$(k_x, k_y, k_z) \rightarrow (k_\perp \cos(\phi), k_\perp \sin(\phi), k_{//})$$

$$d^3 \mathbf{k} \rightarrow k_\perp dk_\perp dk_{//} d\phi$$

with $k_\perp$ the component perpendicular and $k_{//}$ the component parallel to the line of sight.

$$\xi_{g+} = -\frac{C_1 b_g a^3 \bar{\rho}(z)}{D(z)} \int \frac{dk_\perp dk_{//} d\phi}{(2\pi)^3} e^{i(k_\perp r_\perp \cos(\phi) + k_{//} r_{//})} k_\perp \frac{k_\perp^2 \cos(2\phi)}{k^2} P(k) \tag{35}$$

$\int d(\phi) \cos(2\phi) e^{ik_\perp r_\perp \cos(\phi)}$ can be substituted with a Bessel function: $J_n(x) = \frac{i^{-n}}{\pi} \int_0^\pi d\theta e^{ix \cos(\theta)} \cos(n\theta)$. So in this case the second order Bessel function would fit.

$$- 2\pi J_n(k_\perp r_\perp) = \int_0^{2\pi} d\phi e^{ik_\perp r_\perp \cos(\phi)} \cos(2\phi) \tag{36}$$

This results then in the following:

$$\xi_{g+} = \frac{C_1 b_g a^3 \bar{\rho}(z)}{D(z)} \int \frac{dk_\perp}{(2\pi)^2} k_\perp J_n(k_\perp r_\perp) \int dk_{//} \frac{k_\perp^2}{k^2} P(k) (\cos(k_{//} r_{//}) + i \sin(k_{//} r_{//})) \tag{37}$$

For the last step the integral with the sin function can be omitted, because an odd function integrated from $-\infty$ to ∞ gives zero.

$$\xi_{g+} = \frac{C_1 b_g a^3 \bar{\rho}(z)}{D(z)} \int_0^\infty \frac{dk_\perp}{2\pi^2} k_\perp J_n(k_\perp r_\perp) \int_0^\infty dk_{//} \frac{k_\perp^2}{k^2} P(k) \cos(k_{//} r_{//}) \tag{38}$$

This equation describes the cross-correlation between the galaxy overdensity and the galaxy shapes on large scales according to the LA model.

2.3.3   Correlation with the velocity field

Similar calculations can be done for the cross-correlation function between the velocity field and the galaxy shapes.

$$\xi_{v+} = \langle v(\mathbf{0}) \tilde{\gamma}_+(\mathbf{r}) \rangle \tag{39}$$

Note that in observations only the velocity along the line of sight is measured. The velocities in this thesis are therefore always the component of the velocity vector along the line of sight, see figure 3. On large scales the relation between the velocity field and the overdensity field

is linear and can be derived from the continuity equation. In linear theory the continuity equation in Fourier space is given by (Dodelson, 2003, p.270):

$$\dot{\delta} + ikv = 0 \tag{40}$$

At late times the evolution of the overdensity scales with the growth factor D.

$$v(k, \eta) = \frac{i}{k} \frac{d}{d\eta} \left[\frac{\delta}{D} D \right] \tag{41}$$

η is defined as $\eta = \int_0^t \frac{dt'}{a(t')} = \int_0^a \frac{da'}{a'^2 H(a')}$, which is the total comoving distance that light could have traveled since t=0. This is of course a distance, but because it is monotonically increasing it can be used as a time variable called the conformal time. The derivative $d/d\eta$ can then be written as $a^2 H d/da$ and also the linear growth rate (f) can be substituted:

$$f = \frac{a}{D} \frac{dD}{da} \tag{42}$$

The relation between the velocity and the density becomes:

$$v(\mathbf{k}) = ifaH\frac{1}{k}\delta(\mathbf{k}) \tag{43}$$

Here the velocity is the Fourier component of the velocity parallel to $\mathbf{k}$.
When substituting this expression for the velocity into (39) the correlation function can be calculated in the same way as ξ_{g+} and one gets:

$$
\begin{aligned}
\xi_{v+}(\mathbf{r}) = &\frac{C_1 a^3 \bar{\rho}(z)}{D(z)} fH \int_0^\infty \frac{k_\perp dk_\perp}{2\pi^2} J_2 \left(k_\perp r_\perp \right) \\
&\times \int_0^\infty dk_\parallel \frac{k_\perp^2 k_\parallel}{k^4} P_{\delta\Theta}(k) \sin \left(k_\parallel r_\parallel \right)
\end{aligned}
\tag{44}
$$

Instead of the matter power spectrum $P(k)$ the power spectrum of the cross-correlation of the overdensity and the divergence of the velocity field is used. This is explained in Okumura et al. (2019), the divergence field is defined as $\Theta(\mathbf{k}) = \frac{i\mathbf{k}}{aHf}v(\mathbf{k})$. Than $P_{\delta\Theta}$ is substituted with the following relation similar to (17):

$$\langle \delta(\mathbf{k}')\Theta(\mathbf{k}) \rangle = (2\pi)^3 \delta^3(\mathbf{k} - \mathbf{k}') P_{\delta\Theta} \tag{45}$$

In Okumura et al. (2019) (38) and (44) are analysed and compared with results from simulations, this is discussed in the next section (2.4).

2.3.4   E- and B- modes and defining power spectra

It is often also very useful to look at the power spectrum itself, it being the Fourier transform of the correlation function. For this, another decomposition of the shape is introduced called E and B modes. This decomposition comes from weak lensing statistics where the E modes

describe curl-free modes and the B-modes describe divergence-free modes. The decomposition of the shape in E and B modes is defined as follows:

$$
\begin{aligned}
\gamma_E(\mathbf{k}) &= \gamma_+(\mathbf{k})\cos 2\phi + \gamma_\times(\mathbf{k})\sin 2\phi \\
\gamma_B(\mathbf{k}) &= -\gamma_+(\mathbf{k})\sin 2\phi + \gamma_\times(\mathbf{k})\cos 2\phi
\end{aligned}
\tag{46}
$$

With the angle defined as $\phi = \tan^{-1}(\frac{k_x}{k_y})$. In Blazek et al. (2011) the E and B modes for the LA model are calculated and it turns out that the LA model only produces E modes. When talking about the shape of galaxies often the E-mode component of the shape is meant, denoted with subscript E. The power spectra that are required in the further analysis in this thesis are: $P_{gE}, P_{gg}, P_{EE}, P_{vE}, P_{vv}$ and P_{vg} of which P_{gE} and P_{vE} are the most important ones. In general a power spectrum can be calculated with:

$$
P_{xy} = \frac{1}{(2\pi)^3} \int d^3\mathbf{k} \, \langle x(\mathbf{k}')y(\mathbf{k}) \rangle
\tag{47}
$$

with x and y in this case g, E or v. Using (47) the power spectra of the galaxy-shape and velocity-shape correlation are (Kurita et al. 2020):

$$
P_{gE}(k, \mu, z) = -\frac{C_1 b_g \rho_{crit} \Omega_m}{D(z)} (1 - \mu^2) P_{\delta\delta}(k)
\tag{48}
$$

$$
P_{vE}(k, \mu, z) = -\frac{C_1 \rho_{crit} \Omega_m}{D(z)} f a H (1 - \mu^2) \frac{1}{k} P_{\delta\delta}(k, z)
\tag{49}
$$

$P_{\delta\delta}$ is the already known matter power spectrum (17) and μ is the cosine of the angle between the $\mathbf{k}$ and the line of sight, $\mu = \frac{k_z}{k}$. Here a small change of parameters is done in the terms in the front of the expression of the shape (25). $\bar{\rho}a^3$ is substituted with (see 2.1.3 for the used expressions $\Omega_m, \rho_{crit}, \rho_{m,0}$):

$$
\Omega_m \rho_{crit} = \frac{\rho_{m,0}}{\rho_{crit}} \rho_{crit} = \rho_m a^3
$$

2.3.5   Multipole expansion

To get a better grasp of the angular dependence of the statistics described above, one can split the signal of the statistic in multipole moments via a multipole expansion. This is done with the Legendre polynomials as complete basis (see Kurita et al. 2020):

$$
P_{XY}^{(\ell)}(k) \equiv \frac{2\ell + 1}{2} \int_{-1}^{1} d\mu \mathcal{L}_\ell(\mu) P_{XY}(k, \mu)
\tag{50}
$$

Where X and Y are arbitrary labels, ℓ the order of the moment and $\mathcal{L}$ the Legendre polynomial of order ℓ.

2.3.6   Redshift Space Distortions

To be more complete, the effect of Redshift Space Distortions (RSDs) should also be taken into account. These distortions show up when the quantities are described in redshift space.

This is described in chapter 9 of Dodelson (2003). In redshift surveys the distances of galaxies are estimated with the relation between the redshift and the distance (2):

$$\chi_s(z) = \frac{z}{H_0} \tag{51}$$

where χ_s is the comoving distance (2.1.3) in redshift space. However this relation is only valid for low redshift, fortunately the current redshift surveys do not probe that deep. Another problem is that this estimation neglects the peculiar velocities of galaxies. This means that when an overdense region is collapsing (for example forming a cluster) and galaxies move to its center, galaxies on one side of the region are moving away from us, leading to a bigger redshift from those galaxies, which means that they appear further away from us. The galaxies on the other side of the region are moving towards us, so it appears as more closely. The clustering of the galaxies measured in redshift space is therefore distorted. In 1987, Kaiser (Kaiser 1987) was one of the first to study how this effect distorts the clustering signal of the galaxies. In Appendix A from Singh et al. (2015) is mathematically derived how the expression for the shape and the galaxy overdensity are changed in redshift space. It is found that in linear order $\gamma^{red} = \gamma^{real}$ and $\delta_g^{red} = \delta_g^{real}(1 - \frac{f}{b_g}\mu^2)$. While the cross-correlation of the velocity and the shape on linear order is not influenced by RSDs, the cross-correlation of the galaxy density and the shape, is. The galaxy density part contributes this extra $(1 - \frac{f}{b_g}\mu^2)$ term, which leads to the following power spectrum:

$$P_{gE}^{red}(k,\mu,z) = -\frac{C_1 b_g \rho_{crit}\Omega_m}{D(z)}(1-\mu)(1 - \frac{f}{b_g}\mu^2)P_{\delta\delta}(k) \tag{52}$$

2.3.7 A small note on beyond the LA model

For scales smaller than ~ 10Mpc the LA model is no longer valid (see Singh et al. 2015). On scales between $1 - 10$Mpc the LA model power spectrum can be replaced with the non-linear power spectrum from the non-linear linear alignment model (NLA-model). Which is derived with perturbative methods (see Bridle and King 2007, Hirata et al. 2007). For even smaller scales a model called the Halo model can be used (described in Schneider and Bridle 2010). This model assumes that dark matter halos in our universe have a galaxy cluster/group at the center with the alignment of their shapes relative to the halo. Satellite galaxies then tend to point to the center of this halo. An elaborate description of this model is out of the scope of this thesis since the predictions are focused on large scales.

2.4 Velocity-shape correlation

In most literature, intrinsic alignment is studied in relation to the cosmic density fields on large scales. However Okumura et al. (2019) is one of the first to describe the relation between intrinsic alignments with the cosmic velocity field. Although the effects of intrinsic alignments with the velocity field are similar to those with the density field, the alignment with the velocity field is expected to be up to scales larger than with the density field ($r \gg 100h^{-1}\mathrm{Mpc}$). This is because of the linear relation between the velocity and the density in Fourier space (43), in which the velocity is proportional to the density divided by k, the wave number. Small k, which implies large scales, would give an enhancement of the velocity with respect to the density. In the paper a description of these velocity statistics is given and they also work out the linear alignment model for velocity-shape correlation as described in section 2.3. To analyse their derived statistics they perform a series of large N-body simulations which uses ΛCDM cosmology. Similar simulations are done in the follow up and companion papers Okumura et al. (2020) and Okumura and Taruya (2020), however there the multipole expansion (50) is studied. Going deep into these simulations is out of the scope of this thesis, but in this section a couple of their results are described, to be able to compare them with the results in this thesis.

One of the first results is the comparison between the correlation function of the correlation between the density field and the ellipticity and the correlation between the density weighted velocity field (p_m) and the ellipticity, shown in the figure 2 and 6 produced in Okumura et al. (2019). When looking at figure 2 in Okumura et al. (2019) the density and velocity fields are sampled by dark matter and the shape by clusters. In figure 6 of this paper the fields are sampled by galaxies and clusters. The inset in the plots shows the BAO scale, only for the density-shape correlation.

From these figures a few things about velocity-shape correlation in relation to density-shape correlation can be noted.

- The signal of the velocity-shape correlation is larger than that of density-shape correlation on all the scales. In particular on large scales ($> 100h^{-1}\mathrm{Mpc}$) this difference is enlarged as expected.

- The simulation data points in good agreement with the linear alignment model for velocity-shape correlation from a scale of $> 50h^{-1}\mathrm{Mpc}$ and for the density-shape correlation from a scale of $> 25h^{-1}\mathrm{Mpc}$. This indicates that it could be expected that the correlation functions from real data will also more or less follow the LA-model for the larger scales.

- The deviations due to the different used tracers for the underlying fields are minimal for the velocity-shape correlation. In this thesis galaxies are used as tracer of the velocity field, this should then be comparable to dark matter or clusters as tracer. The plots in which the fields are sampled by galaxies and clusters, a higher signal for the density-shape correlation is shown.

- The non-linear model gives a better agreement with the simulation data points on BAO scale shown in the insets. The BAO wiggle in the velocity-shape correlation is

quite suppressed. However in figure 12 the density weighted velocity-shape correlation is multiplied with $r^{1.3}$ which amplifies the suppressed BAO wiggles. Here it can be seen that the points from the simulation follows the NLA model (2.3.7) with BAO signal best. In this way velocity-shape correlation can be used to extract information of BAOs.

In the paper of Okumura and Taruya (2020) they look at the multipole expansion of the LA model for the density-shape correlation and the velocity-shape correlation. In figure 2 they show the plots for the 0th, 2nd, and 4th order poles of the density-shape correlation and the 1st and 3rd order poles of the velocity-shape correlation. For the density-shape correlation both the models in real and redshift space are plotted. From these plots the following can be concluded:

- For both correlations the first two non-zero poles give the same but opposite signal in real space. Higher poles than the octupole for the velocity-shape correlations are zero.

- In linear theory the velocity shape correlation is not affected by RSDs (2.3.6), they are not plotted. For the density-shape correlations the signals in real and redshift space do differ. The hexadecapole is zero in real space, it is not in redshift space.

In the paper of Okumura et al. (2020) they compare this multipole model with the results from the simulation. The results are shown in figure 2 and 5. Again the multipoles of 0th, 2nd and 4th order for the density-shape correlation are plotted in real and redshift space together with the simulation points. The same is done for the velocity-shape correlation for the 1st, 3rd and 5th order poles. In figure 2 the results are calculated with a halo mass of over $10^{13} M_\odot$[10] and in figure 5 with a halo mass of over $10^{14} M_\odot$.
It must be noted that instead of looking at the density-shape correlation, the halo-shape correlation is taken. These two differ on linear scale with a constant halo bias term. The following points can again be noted from these results:

- The points from the simulation are in good agreement with the multipole LA model at large scales for both correlations. This is therefore also expected when measuring the different poles in real data.

- In linear theory velocity-shape correlation is not affected by RSDs. On large scales there is also not much of a deviation between the simulation data points in real and redshift space. However on small scales velocity-shape correlation is affected by RSDs which is also depicted in the plot.

The results pointed out above are kept in mind when analysing and checking the results of the forecast to estimate the measurability of velocity-shape correlation in real data.

---

[10]$M_\odot$ stands for Solar mass, the mass expressed in the mass of the Sun. $M_\odot = 1.9891 \times 10^{30}$kg

2.5 Reconstructing velocities

For doing a prediction about the measurability of the velocity-shape correlation, a method to calculate the velocity field is needed. This can be done by making a reconstruction of the large scale velocity field.

In 2.3.3 it was already shown that on large scales the relation between the velocity and the overdensity in Fourier space is linear (43). One way to reconstruct this velocity field is with the kinetic Sunyaev Zeldovich effect (kSZ). With this method the radial velocity and the noise of this field can be constructed, which is the component of the velocity in the radial direction.

$$v_r(\mathbf{k}) = \frac{ik_r}{k}v(\mathbf{k}) = i\mu v(\mathbf{k}) \tag{53}$$

Where $\mu = \frac{k_r}{k}$ is still the cosine of the angle between wavevector $\mathbf{k}$ and line of sight, here denoted as the radial direction. The linear relation between the radial velocity and the density can be written as:

$$v_r(\mathbf{k}) = \mu\frac{faH}{k}\delta_m(\mathbf{k}) \tag{54}$$

The kSZ effect can be measured when comparing galaxy surveys with the map of the CMB. It is based on the following physical process. When a galaxy has a peculiar velocity, the electrons in for example the gasses of a galaxy, have a velocity aside the random thermal movements. Photons from the CMB that are coming by, are scattered by these electrons in a process that can be seen as inverse Compton scattering. Because the electrons have a velocity on top of their thermal movements, this scattering is not elastic and an energy shift takes place. This leads to a Doppler shift of the CMB photons which can be measured in the CMB spectrum.

Many different statistics are proposed to reconstruct this effect from combining galaxy surveys with the CMB spectrum. In Smith et al. (2018) these different statistics are described and they show that those are all mathematically equivalent. One of those statistics is deriving the reconstructed radial velocity term and the noise from what is called the bispectrum. The bispectrum can be seen as the power spectrum from a correlation function that correlates three variables. In the case of the kSZ effect, combining two galaxy field variables with a CMB variable. In (Smith et al., 2018, p.15-16) the terms for the reconstructed radial velocity, $\hat{v}_r$, and its noise spectrum, N_{v_r} are derived, resulting in:

$$\hat{v}_r\left(k_L\right) = N_{v_r}\left(k_L\right)\frac{K_*}{\chi_*^2}\int\frac{d^3k_S}{(2\pi)^3}\frac{d^2\mathbf{l}}{(2\pi)^2}\frac{P_{ge}\left(k_S\right)}{P_{gg}^{\text{tot}}\left(k_S\right)C_l^{TT,\text{ tot}}}\left(\delta_g^*\left(k_S\right)T^*(\mathbf{l})\right)(2\pi)^3\delta^3\left(k_L + k_S + \frac{\mathbf{l}}{\chi_*}\right)$$

$$N_{v_r}(k_L) = \frac{\chi_*^4}{K_*^2}\left[\int\frac{d^3k_S}{(2\pi)^3}\frac{d^2\mathbf{l}}{(2\pi)^2}\frac{P_{ge}(k_S)^2}{P_{gg}^{\text{tot}}\left(k_S\right)C_l^{TT,\text{ tot}}}(2\pi)^3\delta^3\left(k_L + k_S + \frac{\mathbf{l}}{\chi_*}\right)\right]^{-1}.$$

$$= \frac{\chi_*^2}{K_*^2}\left[\int\frac{k_Sdk_S}{2\pi}\left(\frac{P_{ge}\left(k_S\right)^2}{P_{gg}^{\text{tot}}\left(k_S\right)C_l^{TT,\text{ tot}}}\right)_{l=k_S\chi_*}\right]^{-1}$$

$$\tag{55}$$

Where $k_L \ll k_S$ are respectively the large scale and small scale wavenumbers. P_{ge} the small scale power spectrum of the galaxy density and the electron density and P_{gg} is the

powerspectrum of the auto-correlation between galaxy positions, both can be calculated with the halo model (2.3.7). $T(l)$ describes the anisotropy in the kSZ bispectrum and $C_l^{TT,tot}$ the total CMB power spectrum. δ_g^* is the galaxy overdensity evaluated at redshift z_* and δ^3 denotes the Dirac delta. χ_* is the comoving distance up to redshift z_*. K_* is the kSZ radial weight function in units μK- Mpc^{-1}:

$$K(z_*) = -T_{CMB}\sigma_T n_{e,0} x_e(z_*) e^{-\tau(z_*)}(1 + z_*)^2 \tag{56}$$

With T_{CMB} the CMB temperature, σ_T the Thomson cross section, $n_{e,0}$ the present time electron number density, x_e the position of electrons and τ the optical dept.
Luckily, on large scales the reconstructed radial velocity can be well described by (54). However $\hat{v}_r$ will be a biased estimator of v_r so a bias need to be introduced:

$$\hat{v}_r = b_v v_r \tag{57}$$

The kSZ velocity field reconstructs the velocity field op to a factor b_v which is not known in advance and must be marginalized. In combination with above noise power spectrum, this reconstructed velocity can be used to calculate the needed correlation functions.
In principle this noise power spectrum can be calculated by using the expressions for the small scale electron-matter power spectrum P_{ge} and the galaxy-galaxy power spectrum P_{gg} from the Halo model (Smith et al., 2018, p.33). Also the Cosmic Microwave Background (CMB) power spectrum C_l^{TT} and the weight function K_* with optical dept are needed. Because this is a bit out of the scope of this thesis, an approximation for the value of this noise power spectrum is used. This is possible because the noise approaches a constant on large scales(Smith et al., 2018, p4). In the article Zhu et al. (2020) they looked at how to use a reconstruction of the velocity of galaxies with kSZ for improving the reconstruction of the displacement field which is used to get the linear Baryon Acoustic Oscillation (BAO) signal. The details of this calculation are not relevant here, but they use the linear relation (on large scales) between the velocity and this displacement field ψ

$$\mathbf{v} = afH\psi \tag{58}$$

and take for the noise levels $N_{v_r}/(afH)^2 = 10^6, 10^7\,h^{-5}\text{Mpc}^5$. These levels are approximately what can be achieved when using a CMB experiment for the kSZ calculation with a white noise of $6\,\mu\text{K} - \text{arcmin}$ and a 1.5arcmin beam. The number density of the used galaxy survey was respectively $\bar{n} = 10^{-3}\,h^3\text{Mpc}^{-3}$, $\bar{n} = 10^{-4}\,h^3\text{Mpc}^{-3}$ (Zhu et al., 2020, p8). If the used galaxy survey satisfies these number densities and implicitly using this kind of CMB experiment, the noise levels can be adopted. To get the velocity noise, this noise level can be divided by $(afH)^2$. In the paper (Zhu et al., 2020, p9) they find that $N_{v_r}/(afH)^2 = 10^6, 10^7\,h^{-5}\text{Mpc}^5$ are the velocity noise levels obtained by cross correlating the DESI ELG/LRG survey (DESI Collaboration et al. 2016) with number density $\bar{n} = 10^{-4}h^3\text{Mpc}^{-3}$ and the survey SDSS-MGS (Strauss et al. 2002) with number density $\bar{n} = 10^{-3}h^3\text{Mpc}^{-3}$ with the CMB observations from the Simons Observatory (Simons Observatory Collaboration et al. 2019).

2.6 Fisher forecast

As discussed before it is the aim to find out if the velocity-shape correlation described in Okumura et al. (2019) is measurable with the data of galaxies we have today or in the near future. For achieving this, it is convenient to execute a Fisher forecast calculation, relating on the theory of (Dodelson, 2003, Ch.11). The Fisher matrix formalism is a method to calculate how well the experiment can constrain the parameters of the model you are using. This can be explained in the following way; a Fisher matrix is a measurement of the curvature of the likelihood functions $\mathcal{L}$ from the model parameters. The likelihood function describes the probability of getting certain data given an underlying theory. Imagine the likelihood function of parameter α of which α_0 is the best fit value. The likelihood function would then be peaked around α_0 and the width of the likelihood function gives the uncertainty in the parameter α. When Taylor expanding the likelihood function around α_0 one gets:

$$\mathcal{L}(\alpha) \approx \mathcal{L}(\alpha_0) + \left(\frac{\partial \mathcal{L}}{\partial \alpha}\right)_{\alpha_0} (\alpha - \alpha_0) + \frac{1}{2}\left(\frac{\partial^2 \mathcal{L}}{\partial \alpha^2}\right)_{\alpha_0} (\alpha - \alpha_0)^2 + .. \tag{59}$$

The first derivative is zero because α_0 is the position of the peak in the likelihood function. The first information is therefore hold by the second derivative. However the function is now approximated by a parabola, a better fit would be a Gaussian which can be achieved by looking at the second derivative of the natural logarithm of the likelihood function. This second derivative of $\ln \mathcal{L}$ describes the curvature and thereby the width of the likelihood function and is defined as the Fisher value, with multiple parameters this gives the Fisher matrix:

$$F_{\mu\nu} = -\frac{\partial^2(\ln \mathcal{L})}{\partial \alpha_\mu \alpha_\nu} \tag{60}$$

With μ, ν indices for the different parameters. The greater the Fisher value for a parameter the better the constraints for the parameter value. The specific expression for the Fisher matrix depends on the expression of the likelihood function which then again depends on the used model for the theory. The advantage of this method is that it gives a prediction of the usefulness of your model before doing an experiment. Keeping in mind that it gives the best possible outcome, not necessarily the outcome of the experiment. The calculations from this section and upcoming section are done in Python with the latest version (v2.1.0) of the Core Cosmology Library (Chisari et al. 2019), see A.

The Fisher matrix for cosmological parameters is given by (Taruya and Okumura, 2020, p.2):

$$F_{i,j} = \frac{V_{survey}}{(2\pi)^2} \int_{k_{min}}^{k_{max}} dk \, k^2 \int_{-1}^{1} d\mu \sum_{a,b} \frac{\partial P_a(k,\mu)}{\partial \theta_i} \frac{1}{\sigma_{ab}} \frac{\partial P_b(k,\mu)}{\partial \theta_j} \tag{61}$$

Where P_a, P_b are the power spectra that contain the cosmological information of the model with a and b for example gE, gg, EE or v_rE correlations. θ_i are the parameters that characterise the power spectra. The derivatives of the power spectra are multiplied with one divided by the covariance matrix (σ_{ab}) of the power spectra and after summing, integrated μ and k. The volume and the minimum and maximum wave numbers come from the particular survey.

For the velocity-shape correlation the cosmological information is embedded in the P_{v_rE}

power spectrum. The normalization parameter C_1 gives the strength of the alignment. It depends on the properties of the galaxies in the measured sample, as the luminosity, mass, redshift and cosmological parameters. It gives information about the measurability of this correlation. By constructing the Fisher forecast for this power spectrum and parameter and inverting the matrix, the variance of C_1 is calculated. From the variance the fractional error for C_1 can be derived. The fractional error gives how well this correlation can constrain the alignment strength. If it turns out the constraining of this correlation is promising, it can be expected that intrinsic alignment with the velocity field can be measured. In this case the Fisher matrix can be calculated with:

$$F_{C_1 C_1} = \frac{V_{survey}}{(2\pi)^2} \int_{k_{min}}^{k_{max}} dk \, k^2 \int_{-1}^{1} d\mu \left(\frac{\partial P_{v_r E}(k, \mu)}{\partial C_1} \right)^2 \frac{1}{\sigma^2_{P_{v_r E}, P_{v_r E}}} \tag{62}$$

Following the line of Taruya and Okumura (2020) instead of just looking at parameter C_1, $\widetilde{C_1} = \frac{C_1 \rho_{crit} \Omega_m}{D(z)}$ is taken, which keeps the calculation more compact and the result are the same. This is because ρ_{crit}, Ω_m and $D(z)$ follow from the cosmological model that is used, see 2.1.4. In some references (for example Singh et al. 2015, Joachimi et al. 2011) they choose to fix the value of $C_1 \rho_{crit}$ by matching the amplitude of the model to the observations and introduce an extra arbitrary amplitude parameter A_I which can be varied and depends on z and on the luminosity with a power law (see Singh et al. 2015). In others, like the paper used for doing this calculation; Taruya and Okumura (2020), they absorb this into an arbitrary normalisation parameter $\widetilde{C_1}(z)$ which is z dependent, the latter will be followed here. Occasionally (see 3.3) $-\widetilde{C_1}$ is called b_I, the linear alignment bias. With this $\widetilde{C_1}$ equation (62) becomes:

$$F_{\widetilde{C_1} \widetilde{C_1}} = \frac{V_{survey}}{(2\pi)^2} \int_{k_{min}}^{k_{max}} dk \, k^2 \int_{-1}^{1} d\mu \left(\frac{\partial P_{v_r E}(k, \mu)}{\partial \widetilde{C_1}} \right)^2 \frac{1}{\sigma^2_{P_{v_r E}, P_{v_r E}}} \tag{63}$$

Because this Fisher forecast is done for one power spectrum and one parameter, a 1,1-dimensional matrix is obtained, in this case the terms Fisher matrix and Fisher value are interchangeable.

The power spectrum of the correlation between the velocity and the shape is given by (49). However the kSZ effect is used to reconstruct the radial velocity field which lead to the extra μ and b_v terms to relate the velocity to the reconstructed radial velocity (see 2.5). This gives the following power spectrum:

$$P_{v_r E}(k, \mu, z) = -\widetilde{C_1}(z) b_v f a H (1 - \mu^2) \mu \frac{1}{k} P_{\delta\delta}(k, z) \tag{64}$$

So (64) gives the final expression for the power spectrum. With similar calculation the auto power spectra of the ellipticity and the velocity can be obtained.

$$P_{v_r v_r}(k, \mu, z) = \left(\frac{\mu b_v f a H}{k} \right)^2 P_{\delta\delta}(k, z) \tag{65}$$

$$P_{EE}(k, \mu, z) = \left[\widetilde{C_1}(z)(1 - \mu^2) \right]^2 P_{\delta\delta}(k, z) \tag{66}$$

For the elements from covariance matrix needed for the Fisher value, Gaussian covariance is used. This is a reasonable approximation because this calculation is done in the linear regime. From the covariance matrix given in (Taruya and Okumura, 2020, p.2) it can be derived that the variance is given by:

$$\sigma^2_{P_{v_r E} P_{v_r E}} = \tilde{P}_{EE} \tilde{P}_{v_r v_r} + P^2_{v_r E} \tag{67}$$

The tilde means the power spectrum itself with the contribution of the noise. Specifically: $\tilde{P}_{EE} = P_{EE} + \frac{\sigma^2_\gamma}{\bar{n}_{gal}}$ and $\tilde{P}_{v_r v_r} = P_{v_r v_r} + N_{vv}$, where $\bar{n}_{gal}$ is the mean number density of galaxies, σ_γ the scatter in the intrinsic shape per component, mainly due to the measurement uncertainty and N_{vv} the noise power spectrum. This noise power spectrum is given by (Smith et al., 2018, p.20):

$$N^{rec}_{vv}(k_L, \mu) = \mu^{-2} N_{v_r} \tag{68}$$

As described in (2.5) the velocity power spectrum N_{v_r} can be approximated by $N_{v_r}/(afH)^2 = 10^6 h^{-5} \text{Mpc}^5$. This means that a CMB experiment is used as described in (2.5) and the used galaxy survey must have a number density of $\bar{n} = 10^{-3} h^{-3} \text{Mpc}^3$.

For this Fisher calculation the predicted values for the upcoming LSST survey (Ivezić et al. 2019) are used, see A.

	average redshift	red fraction	$\bar{n}_{gal}(\text{Mpc}^{-3})$	$V_{survey}(\text{Mpc}^3)$	$\widetilde{C1}$
LSST	1.0	0.1214	6.9×10^{-3}	113.4×10^9	0.027

Table 1: Prediction for LSST data

This galaxy number density is in accordance with the number density needed to adopt the noise level from Zhu et al. (2020). In the Fisher calculation the galaxy number density will be multiplied by the red fraction, this is fraction of your galaxy sample that are red galaxies. The filtering of these galaxies is applied because there is evidence for the alignment of galaxies shapes for red galaxies, but not for blue galaxies (2.1.4). Furthermore choosing the values for $k_{min} = 2\pi/V^{\frac{1}{3}}_{survey} \ h \ \text{Mpc}^{-1}$ and $k_{max} = 1 \ h \ \text{Mpc}^{-1}$ to stay safely in large scales where linear theory can be applied. Following Taruya and Okumura (2020) for taking $\sigma_\gamma = 0.3$ as this value being a typical shape noise. The bias b_v of the velocity reconstruction is set to 1. When differentiating (64) to $\widetilde{C}_1$ and plugging into (63) with the other values from above, the Fisher matrix becomes:

$$F_{\widetilde{C}_1 \widetilde{C}_1} = \frac{V_{survey}}{(2\pi)^2} \int_{k_{min}}^{k_{max}} dk \, k^2 \int_{-1}^{1} d\mu \left[(-1) a b_v f H (1-\mu^2) \mu \frac{1}{k} P_{\delta\delta}(k) \right]^2$$

$$\times \frac{1}{(P_{EE} + \frac{\sigma^2_\gamma}{\bar{n}_{gal}})(P_{v_r v_r} + N_{vv}) + \left[(-1) \widetilde{C}_1(z) b_v f a H (1-\mu^2) \mu \frac{1}{k} P_{\delta\delta}(k) \right]^2} \tag{69}$$

The inverse of the Fisher matrix gives the covariance matrix of the parameters. In this case, the Fisher matrix is a 1,1 dimensional matrix and the inverse is just $1/F_{\widetilde{C}_1 \widetilde{C}_1}$, which is

the variance of the parameter $\widetilde{C_1}$. To calculate the fractional error of $\widetilde{C_1}$, the square root to the variance is divided by the value of $\widetilde{C_1}$ itself. The same forecast is done for P_{gE} with a galaxy bias of 1.7 (Smith et al. 2018, p.17) for which alignment signals are already measured in for example the SDSS LOWZ survey in Singh et al. (2015).

The problem with this calculation is that it can not be fairly compared with the simulation results in section 2.4 and a calculation of the signal to noise ratio of the power spectra itself. This is because to implement the angular information of the power spectra, the multipole formalism is needed as given by (50). When averaging (64) over μ by taking the integral over μ from -1 to 1 to take the angular information into account, this would give zero. (64) is namely an anti-symmetric function in μ. With the multipole formalism the angular information is separated in the different poles by multiplying with the Legendre polynomials. Due to this multiplication, one gets a symmetric function in μ for specific orders of the polynomials, that can be integrated.

To get results that can be compared, this Fisher calculation is done with the multipole formalism. This changes the Fisher formalism from above in the following way:

- The power spectra $P_{v_r E}$ and P_{gE} for the two Fisher calculations are replaced by their multipole expressions (50) for the dipole and the monopole respectively.

$$P_{v_r E}^{(1)}(k) \equiv \frac{3}{2} \int_{-1}^{1} d\mu \mathcal{L}_1(\mu) P_{v_r E}(k, \mu) \tag{70}$$

$$P_{gE}^{(0)}(k) \equiv \frac{1}{2} \int_{-1}^{1} d\mu \mathcal{L}_0(\mu) P_{gE}(k, \mu) \tag{71}$$

- The covariance value for the power spectra is multiplied with the corresponding Legendre polynomials and integrated over μ to get the multipole version of the covariance. This is based on the multipole formalism of the Gaussian covariance from (Kurita et al., 2020, p11).

$$\mathbf{C}_{11}^{P_{v_r E}^{(1)}} = \sigma^2_{P_{v_r E}^{(1)}, P_{v_r E}^{(1)}} \equiv 9 \int_{-1}^{1} d\mu \mathcal{L}_1(\mu) \mathcal{L}_1(\mu)$$
$$\times \left[P_{v_r E}^2(k, \mu) + \widetilde{P}_{v_r v_r}(k, \mu) \widetilde{P}_{EE}(k, \mu) \right] \tag{72}$$

$$\mathbf{C}_{00}^{P_{gE}^{(0)}} = \sigma^2_{P_{gE}^{(1)}, P_{gE}^{(1)}} \equiv \int_{-1}^{1} d\mu \mathcal{L}_0(\mu) \mathcal{L}_0(\mu)$$
$$\times \left[P_{gE}^2(k, \mu) + \widetilde{P}_{gg}(k, \mu) \widetilde{P}_{EE}(k, \mu) \right] \tag{73}$$

In the expressions above the $\frac{(2\pi/L)^3}{4\pi k_i^2 \Delta k}$ from Kurita et al. (2020) is omitted, because it is already present in the expression for the Fisher value. This is because in the paper, one divided by the covariance terms are summed over k_i. In the Fisher expression there is an integral over k. So Δk can be interpret as dk and k_i^2 as k^2. The term in the front of the integral in the Fisher expression is the same as $\left(\frac{(2\pi/L)^3}{4\pi} \right)^{-1}$.

- The integral over μ in the Fisher expression is now already done in the multipole expressions, so only the integration over k is left.

$$F_{\widetilde{C_1}\widetilde{C_1}} = \frac{V_{\text{survey}}}{(2\pi)^2} \int_{k_{\min}}^{k_{\max}} dk\, k^2 \left(\frac{\partial P_{v_r E}^{(1)}(k)}{\partial \widetilde{C1}}\right)^2 \frac{1}{\sigma^2_{P_{v_r E}^{(1)}, P_{v_r E}^{(1)}}} \tag{74}$$

$$F_{\widetilde{C_1}\widetilde{C_1}} = \frac{V_{\text{survey}}}{(2\pi)^2} \int_{k_{\min}}^{k_{\max}} dk\, k^2 \left(\frac{\partial P_{gE}^{(0)}(k)}{\partial \widetilde{C1}}\right)^2 \frac{1}{\sigma^2_{P_{gE}^{(0)}, P_{gE}^{(0)}}} \tag{75}$$

This Fisher forecast results in a fractional error of $\delta\widetilde{C_1}/\widetilde{C_1} = 0.022$ with respect to the velocity shape correlation and a fractional error of $\delta\widetilde{C_1}/\widetilde{C_1} = 0.0011$ for the galaxy shape correlation.

Apart from the fractional error of $\widetilde{C_1}$, it is also useful to look at the power spectrum with its error bars. This should be consistent with the measurability of the signal. By plotting the dipole signal of (64) with errorbars from the square root of the variance (72), the following plot is obtained with a signal to noise ratio of 263[11], see figure 4. For comparison also the monopole of P_{gE} with its errorbars is plotted. This signal has a signal to noise ratio of 349.

The high signal to noise value of $P_{v_r E}$ tells that this signal has a good measurability. From the plot it can be seen that the signal of the velocity shape correlation is higher than that of the galaxy shape correlation, at most at the large scales of $\sim k = 10^{-2}$, which agrees with the results of Okumura et al. (2019). For scales $\ll k = 10^{-2}$ the error of the power spectrum is too big to be able to compare the two signals. A more accurate calculation is needed to make this distinction.

	fractional error $\delta\widetilde{C_1}$	Signal to noise ratio power spectrum
$v_r E$ correlation	0.022	263
gE correlation	0.011	359

Table 2: Results Fisher forecast $P_{v_r E}$, P_{gE}

The difference in the signal to noise of the power spectra is consistent with the difference in the fractional errors of $\widetilde{C_1}$. Both fractional errors are quite small. The galaxy-shape correlation is already measured for Luminous Red Galaxies (2.1.4) and the uncertainty on this correlation is lower, seen from the lower signal to noise. Still the signal to noise for the velocity-shape correlation is in the same order and the fractional error for $\widetilde{C1}$ is quite small. From this, it can be predicted that the velocity-shape correlation probably can be measured

---

[11]In the plots, the power spectra are multiplied by -1 so they are positive. This is done for clarity and to be able to plot them logarithmic. This has no consequences for further analysis, but it is important to keep in mind
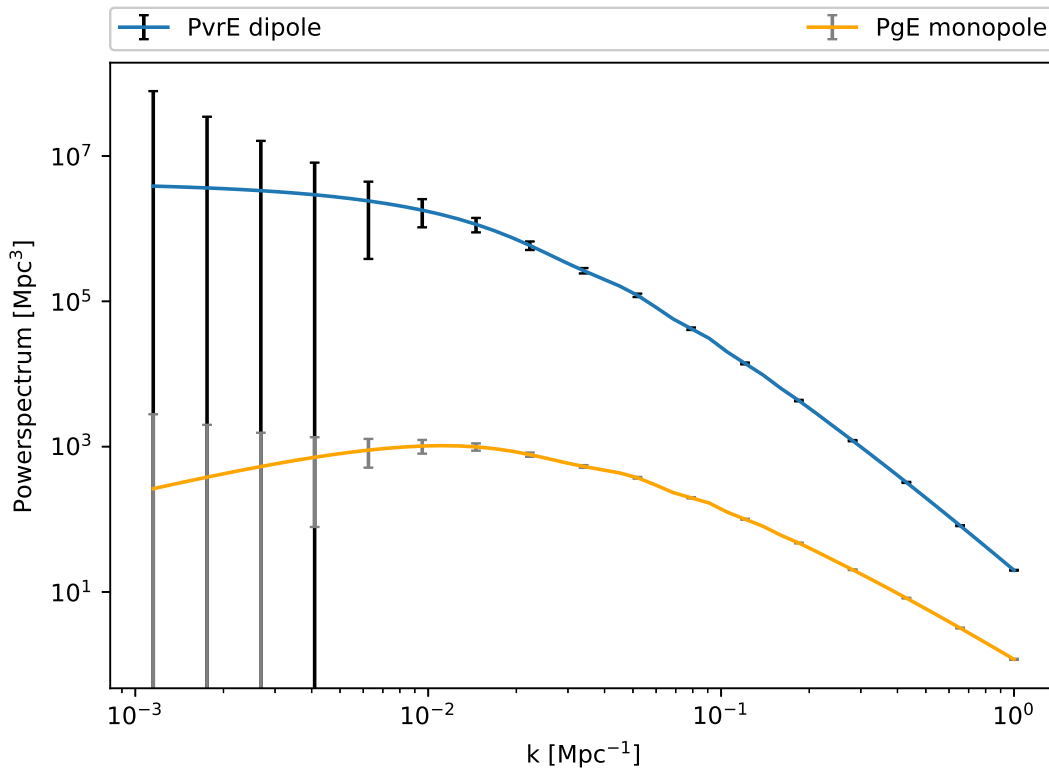
Figure 4: dipole of P_{vrE} and the monopole of P_{gE}, data from LSST-Y1.

in upcoming surveys like LSST with a bit more uncertainty than for the galaxy-shape correlation.

However, in this prediction gravitational lensing effects are ignored. In for example Singh et al. (2015) this is also done but they used the SDSS LOWZ survey which probes till a redshift of $z \sim 0.36$. Here, data from the LSST survey was used which probes till $z \sim 1$. The higher the redshift, the more gravitational lensing contamination because there are more foreground 'lens' galaxies in the survey. So for LOWZ, lensing effects are negligible, for LSST is this not the case. The results above should therefore actually be corrected for gravitational lensing which also alters the observed shape of galaxies (20). One can get around the gravitational lensing contamination when a spectroscopic survey is used. Large sky surveys such as LSST often use photometry to determine the redshift of objects. With photometry the brightness of an object viewed through different filters and the estimate is less good than with spectroscopy (2.1.1). Although it is also less time consuming and often sufficient. Because the redshift measurements with spectroscopy are more accurate, one can select galaxies more precisely, ensuring they are around the same redshift. In this case the shear of the galaxy shapes can only be caused by intrinsic alignment effects because the galaxies are close together so would not lens one another. When selecting the galaxies this way the gravitational lensing effects are eliminated. 4MOST (Richard et al. 2019) is such a spectroscopic survey and it lies within the LSST survey. When the results for above calculation with 4MOST data

also give promising results, there is a stronger indication for the measurability of velocity-shape correlation.

The values used from LSST in the Fisher forecast (3) are replaced by the values from 4MOST. The number density of this survey is also corresponding with the number density in Zhu et al. (2020), so the estimation of the velocity noise spectrum can be used for this calculation as well.

	average redshift	$\bar{n}_{gal}$ (Mpc^{-3})	V_{survey}(Mpc^3)	$\widetilde{C}_1$
4MOST	0.55	4.5×10^{-3}	0.66×10^9	0.026

Table 3: Prediction for 4MOST data

The following plot for the velocity-shape dipole and galaxy-shape monopole power spectra is obtained.
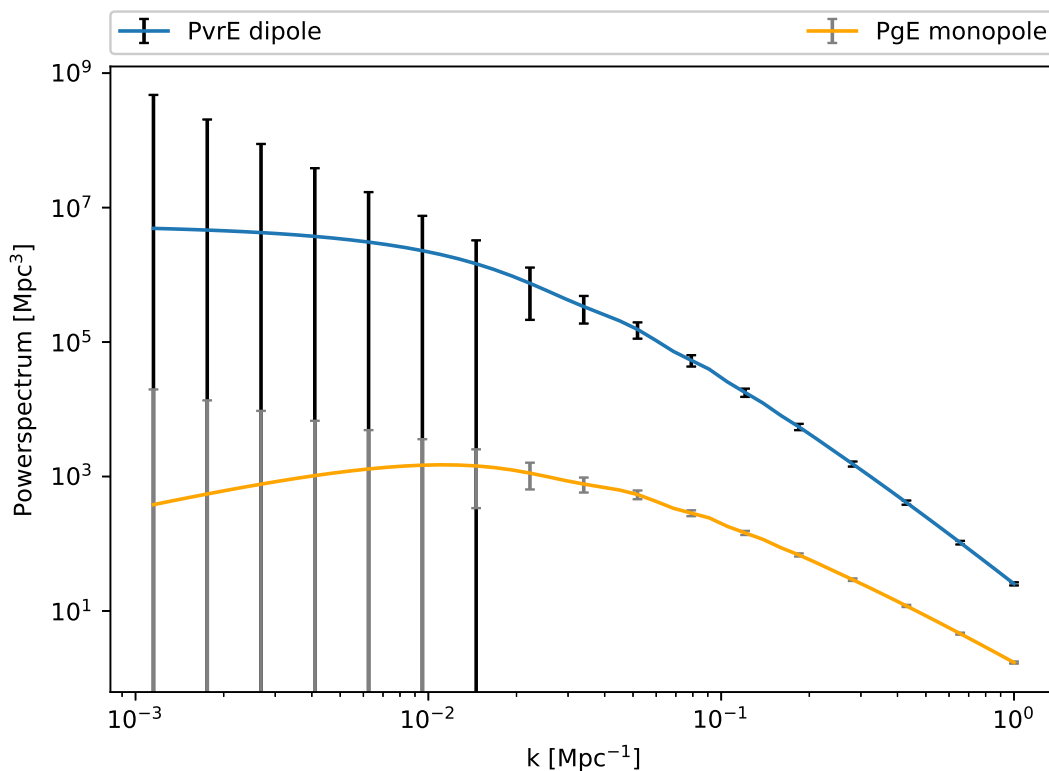

Figure 5: dipole of P_{vrE} and the monopole of P_{gE}, data from 4MOST.

The table gives an overview of the acquired fractional errors of parameter $\widetilde{C}_1$ and the signal to noise of the power spectra.

	fractional error $\delta\widetilde{C}_1$	Signal to noise ratio power spectrum
$v_r E$ correlation	0.11	55
gE correlation	0.058	101

Table 4: Results Fisher forecast $P_{v_r E}$, P_{gE}, data from 4most

The fractional errors for $\widetilde{C}_1$ are larger and the signal to noise of the power spectra is smaller due to larger errors as can be seen in the plot. This could be expected because of the smaller number density and volume of this survey. The fractional errors are still quite small and the signal to noise values are reasonable. The difference in signal to noise of the two power spectra also correspond with the difference in fractional error of the different correlations. All in all the results for this smaller spectroscopic survey are still reasonable which gives a stronger argument for the measurability of the velocity-shape signal.

3 Application

From the previous section it can be stated that velocity-shape correlation can probably be measured with reasonable uncertainties. Now it is time to look at how this correlation can be used, apart from just collecting more data. In the introduction the usefulness of looking at the intrinsic alignment with respect to the velocity field is generally described. In this section a deeper description of applications of measuring velocity-shape correlation is given. Three fields of research and the effect of implementing velocity-shape correlation in the measurements are put forward, followed by a prediction of how velocity-shape correlation can improve the results.

3.1 Selection effects induced by alignment

In the paper Martens et al. (2018) a selection effect due to alignment of galaxies is studied. When observing galaxies, the galaxies parallel to the line of sight are more likely to be observed than the galaxies perpendicular to the line of sight. When a galaxy is along the line of sight, the stars are observed as packed together. This gives a brighter, more compact galaxy which will be observed more easily than the more spread out, less bright galaxies perpendicular to the line of sight. The galaxies along the line of sight are aligned with the tidal field, hence this effect is linked to the intrinsic alignment of galaxies. This effect causes extra anisotropy in the measured galaxy clustering in redshift space (RSDs). This clustering is an important way to probe structure formation in the universe. When this selection effect leaves a significant imprint on the correlation function of these RSDs, one needs to correct for this effect. In Martens et al. (2018) this effect leads to a significant difference in the alignment amplitude of only radial orientated galaxies relative to only perpendicular orientated galaxies.

There was already a theoretical description of this effect in Hirata (2009). The alignment of large red galaxies with the stretching axis of the tidal field, combined with this observational selection effect will give different observed density modes.
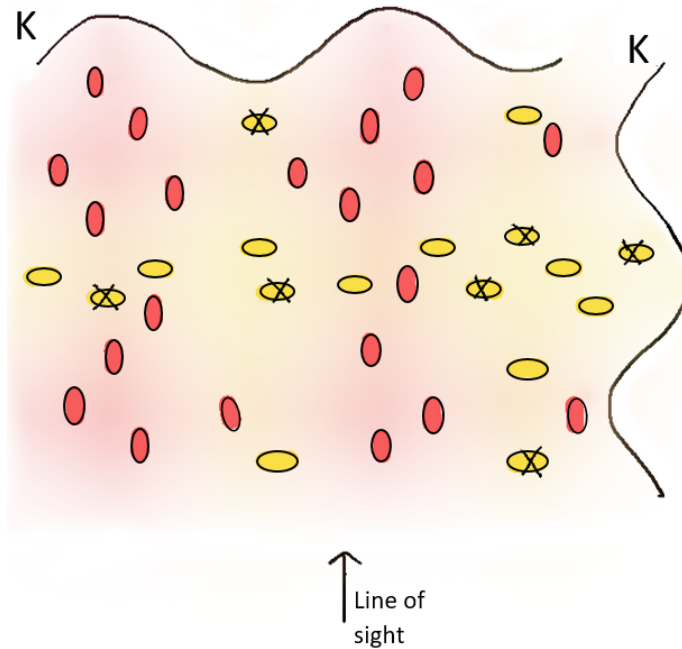
Figure 6: Based on figure 1 from Martens et al. (2018), schematic picture of the selection effect. Galaxies perpendicular(yellow) to the line of sight are harder to observe because their light is spread over a larger area, so a few of those galaxies will not appear when observing. This is exaggerated in this picture by crossing out a few of those galaxies, influencing the measured k-modes.

Figure 6 shows a schematic picture of the situation. The probability of measuring galaxies perpendicular to the line of sight is lower, this is shown as canceling out a few of those galaxies. On top and on the right sight of the picture are particular Fourier modes (k-modes) shown, respectively the perpendicular and parallel. A peak gives at that length scale a high probability for a galaxy to be, so the galaxy density will be higher, hence the more drawn galaxies in the picture. The cancelling out of the perpendicular galaxies will cause the troughs of the perpendicular modes to be even deeper and the peaks of the parallel modes to be damped. The signal of the perpendicular k-modes will therefore increase and the one of the parallel k-modes will decrease, hence the power spectrum in those directions is different. This mimics clustering of galaxies by amplifying the signal in different ways for the parallel and tangential directions. Therefore this effect interferes with the observed clustering due to RSD's that are taken into account in the alignment correlations. If this effect is present it should be taken into account when observing galaxies. Then the measurements of RSDs or effects that are affected by RSDs, like intrinsic alignments, are altered.
In Martens et al. (2018) they show this selection effect is indeed there in the observations. They split the galaxy sample of the SDSS survey in two sub samples, one containing only the galaxies perpendicular to the line of sight and the other one with only the galaxies parallel to the line of sight. Of these sub samples, they measure the clustering of the galaxies to determine the RSD parameters and parameter B, a measure of the strength of the alignment of the galaxies with the tidal field. With the RSD parameters they can test the theoretical

predictions of Hirata (2009). With the B parameter they compare the measurements of the parallel galaxies with the measurements of the perpendicular galaxies to see if they indeed give different outcomes of the alignment strength. Their results turn out to be consistent with the theory and give an evidence for the selection effect.

In Martens et al. (2018) a brief overview of the analysis of Hirata (2009) is given. There they introduce an extra parameter, ϵ, it describes the contribution of the anisotropic selection effect to the galaxy overdensity. In this way the observed galaxy number density at $\mathbf{x}$ in direction $\hat{\mathbf{n}}$ is given by $(1 + \epsilon(\hat{\mathbf{n}} \mid \mathbf{k}))\, n$ with n the galaxy number density if the orientations were randomized. For the galaxy overdensity this gives in linear order

$$\delta_g(\mathbf{k}) = (b + f\mu^2)\delta_m(\mathbf{k}) + \epsilon(\hat{\mathbf{e}}_3 \mid \mathbf{k}) \tag{76}$$

with $\hat{\mathbf{e}}_3$ the line of sight direction. In the linear limit the intrinsic alignments follow the tidal field and therefore ϵ can be expressed as:

$$\epsilon(\hat{\mathbf{n}} \mid \mathbf{x}) = As_{ij}(\mathbf{x})\hat{n}_i\hat{n}_j \tag{77}$$

With A a bias parameter that depends on intrinsic alignment and the selection effects and s_{ij} the dimensionless tidal field; $s_{ij}(\mathbf{x}) = \left[\nabla_i\nabla_j\nabla^{-2} - \frac{1}{3}\delta_{ij}\right]\delta_m(\mathbf{x})$. The galaxy density power spectrum changes from:

$$P_g(\mathbf{k}) = \left[b - f\mu^2\right]^2 P_m(k) \tag{78}$$

to:

$$P_g(\mathbf{k}) = \left[b - \frac{A}{3} + (f + A)\mu^2\right]^2 P_m(k) \tag{79}$$

So the selection effect results in a term compressing the bias. The RSD measurement of f has changed to $(f + A)$. This means that whenever a correlation depends on the galaxy density, this selection effects shows up, for example in the galaxy-shape and galaxy-velocity correlation power spectra.

$$P_{gE}(\mathbf{k}) = -\widetilde{C1}(1 - \mu^2)\left[b - \frac{A}{3} + (f + A)\mu^2\right]P_m(k) \tag{80}$$

$$P_{gv_r} = \left[b - \frac{A}{3} + (f + A)\mu^2\right]b_v f a H \mu \frac{1}{k}P_m(k) \tag{81}$$

The velocity shape (64), shape-shape (66) and velocity-velocity (65) correlation, which only depend on the dark matter over density in linear order, not the galaxy density, stay free of this effect.

However when not taking the linear limit the galaxy shape does depend on the galaxy density (25), so the selection effect does show up in higher order terms for the velocity-shape and shape-shape correlations. When staying in the linear regime (> 10Mpc) the effect is negligible.

This can be useful, usually with RSD measurements the parameter f, the growth rate, is determined. When using galaxy-galaxy, galaxy-shape and/or galaxy-velocity correlation the measurement of f is altered to the measurement of $(f + A)$ due to this observational selection

effect. However when using velocity-shape, shape-shape and/or velocity-velocity correlation in the linear limit to measure f, then this measurement is not affected by the selection effect and just f itself is measured. Combining the three correlation functions with for example a Fisher forecast as described in 2.6 for the correlations with selection effects and correlations without, the expectation will be that this gives a good constraining power for $(f + A)$ and f. With only one way to measure $(f + A)$, different values of A can give the same result for the power spectrum, to there is a degeneracy. When comparing these multiple results for f, the degeneracy in determining A can be broken.

3.2   Scale dependence of intrinsic alignment

In the paper Leonard et al. (2018) is described how the scale dependence of the alignment signal can be constraint by using two measurements of the galaxy shapes. The linear and non linear alignment model work both well to describe the alignment effects on large scales but not work on the small scales. The latter is an active field of research. Insight in the scale dependence of intrinsic alignment enables constructing an improved model.
Earlier in Singh and Mandelbaum (2016) they found that when taking two different shape measurements of galaxies, on a different radial distance from the centre of the galaxy, there is a scale independent multiplicative change in the alignment amplitude. This is because the outer parts of a galaxy are more sensitive to the tidal field because the gravitational attraction of the galaxy itself is weaker than in the more inner parts of the galaxy.
In the paper Leonard et al. (2018) they take advantage of this effect for finding a method to determine the scale dependence of intrinsic alignment on small scales. They take two tangential shear measurements with the same source and lens galaxies, γ_1 and γ_2. The only difference will be the method to estimate the shear. The shear of a galaxy has a weak lensing part and an intrinsic alignment part (20). In the two measurements the lensing part (G) will be the same, the same source and lens galaxies are used, but the measured intrinsic alignment part (I) will be different, because of the two different shear measurement methods.

$$\gamma_1^{obs} = \gamma_1^I + \gamma^G + \gamma^{random} \tag{82}$$

$$\gamma_2^{obs} = \gamma_2^I + \gamma^G + \gamma^{random} \tag{83}$$

Then the lensing contribution can be removed by taking the difference of the two shear measurements. The random contribution to the shape will be averaged out when doing the measurement for many galaxies.

$$\gamma_1^{obs} - \gamma_2^{obs} = \gamma_1^I - \gamma_2^I \tag{84}$$

In this way you only keep the intrinsic alignment measurement on different scales, which can be used to determine the scale dependence. They find that this method improves with respect to already existing methods on two requirements: When the two shape measurements result in greater values of the difference between the intrinsic alignment amplitude of the two different shear estimates and when a greater value of the correlation between the shape noise of each shear estimate is reached.
When there are two different shape measurements of a galaxy which both are done at a different distance from the center of the galaxy, two power spectra of the cross-correlation

with the shape and the galaxy density can be calculated, say P_{gE1} and P_{gE2}. Those power spectra are proportional to the alignment amplitude $P_{gE} \propto A_I$, see (48). From Singh and Mandelbaum (2016) follows that the difference in alignment amplitude for different shape measurements can be tens of percent, which leads to a multiplicative change in the power spectra for all scales. In other words

$$P_{gE1} = c \, P_{gE2} \tag{85}$$

with c a constant. If both power spectra can be modeled with the same model, which is the case in the alignment model, P_{gE1} and P_{gE2} are both the model power spectrum multiplied with a constant factor, say c_1 and c_2. When taking the difference of these two power spectra, one gets:

$$P_{gE1} - P_{gE2} = (c_1 - c_2) \, P_{gE_{model}} = c_g \, P_{gE_{model}} \tag{86}$$

With c_g again a constant and $P_{gE_{model}}$ the model of the power spectrum, see figure 7.
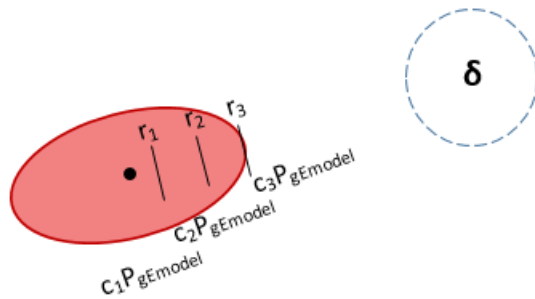

Figure 7: determining scale dependence of the alignment model with different shape measurements at different radii

Comparing these different outcomes for correlation on small scales gives information about how the model behaves at these small scales and thus how it can be improved.
The power spectrum of the velocity shape cross-correlation is also proportional to the alignment amplitude. So using different shape measurements will give a change in the same way:

$$P_{vE1} - P_{vE2} = c_v \, P_{gE_{model}} \tag{87}$$

with c_v a constant. One can also imagine to cross correlate one shape measurement with the velocity and the other with the galaxy density so then the information would be given by

$$P_{vE1} - P_{gE2} = c_{vg} \left(P_{vE_{model}} - P_{gE_{model}} \right) \tag{88}$$

with c_{vg} again a constant. Comparing the prediction of the difference signals could tell what advantages these measurements could give next to more data to construct the scale dependence. Here this is done with a Fisher forecast as in 2.6. An extra parameter α is introduced to describe the change in alignment amplitude when different shape measurements are used. When the difference is taken of the power spectra with different shape measurements, the scaling that than occurs in the signal can be described as:

$$\Delta P_{v_r E} = P_{v_r E, 1} - P_{v_r E, 2} = (1 - \alpha) \, P_{v_r E} \tag{89}$$

Similar for galaxy-shape correlation:

$$\Delta P_{gE} = P_{gE,1} - P_{gE,2} = (1 - \alpha)\, P_{gE} \tag{90}$$

With a Fisher forecast on the combination of those two difference power spectra, the effect of adding velocity-shape correlation on constraining α can be predicted. First a Fisher forecast with the power spectrum P_{gE} to the parameter α is done with the same data and formalism as in 2.6. The following expression is calculated:

$$F_{\alpha\alpha} = \frac{V_{\text{survey}}}{(2\pi)^2} \int_{k_{\min}}^{k_{\max}} dk\; k^2 \left(\frac{\partial P_{gE}^{(0)}(k)}{\partial \alpha} \right)^2 \frac{1}{\sigma^2_{P_{gE}^{(0)}, P_{gE}^{(0)}}} \tag{91}$$

The fractional error of α is then given by taking the square root of the inverse of this Fisher value and dividing it by the value of α. The fiducial value for α is chosen as 0.8 which gives a change in alignment amplitude of 20%. That is in line with the finding of tens of percent change in alignment amplitude for different shape measurements in Singh and Mandelbaum (2016). This gives a fractional error of $\delta\alpha/\alpha = 0.013$.

Now the information of P_{gE} is combined with $P_{v_r E}$ in the Fisher calculation. This means that in calculating the Fisher value, a sum over the different combinations of the power spectra is executed (see 61). Leading to the following expression:

$$F_{\alpha\alpha} = \frac{V_{survey}}{(2\pi)^2} \int_{k_{min}}^{k_{max}} dk\; k^2 \times$$
$$\left[\left(\frac{\partial P_{gE}^{(0)}(k)}{\partial \alpha} \right)^2 \frac{1}{\sigma^2_{P_{gE}^{(0)} P_{gE}^{(0)}}} + 2\frac{\partial P_{gE}^{(0)}(k)}{\partial \alpha} \frac{1}{\sigma_{P_{gE}^{(0)} P_{v_r E}^{(1)}}} \frac{\partial P_{v_r E}^{(1)}(k)}{\partial \alpha} + \left(\frac{\partial P_{v_r E}^{(1)}(k)}{\partial \alpha} \right)^2 \frac{1}{\sigma^2_{P_{v_r E}^{(1)} P_{v_r E}^{(1)}}} \right] \tag{92}$$

The covariance of two cross-correlation power spectra is not implemented in the papers Taruya and Okumura (2020) and Kurita et al. (2020) which were used before to express the covariance term. A more elaborate description of the covariance terms for different power spectra is given by (Duncan et al., 2014, p.4). Here the multipole version of this covariance expression is used:

$$\mathbf{C}_{10} = cov_{P_{v_r E}^{(1)}, P_{gE}^{(0)}} \equiv 3 \int_{-1}^{1} d\mu \mathcal{L}_1(\mu) \mathcal{L}_0(\mu)$$
$$\times \left[P_{gv}(k, \mu) \widetilde{P}_{EE}(k, \mu) + P_{v_r E}(k, \mu)\, P_{gE}(k, \mu) \right] \tag{93}$$

This combining of the power spectra gives a fractional error $\delta\alpha/\alpha = 0.0085$ so significantly smaller with an order of ten. Predicting here that adding the information of velocity-shape correlation to measuring scale dependence with multiple shear measurements could lead to an improvement.

3.3   Measuring non-Gaussianities in the primordial fields with alignments

Inflation is a poorly known period in the evolution of the universe. More information about this period is needed to determine which of the inflation theories is the most promising. Measurement of non-Gaussianities of primordial fields can give this kind of information. In Schmidt et al. (2015) they describe how intrinsic alignments can be related to non-Gaussianity and how it can help to constrain the anisotropic non-Gaussianity coefficient. The correlations between intrinsic galaxy shapes are induced by the tidal field on large scales. Primordial non-Gaussianities cause a scale-dependent imprint on the tidal field. Thus by studying intrinsic alignment, information of non-Gaussianities can be extracted. As it turns out the constraining of the anisotropic non-Gaussianity with using intrinsic alignment is not much better than the already exciting result with using CMB measurements. However the measurement probe smaller scales, so can be seen as complementary to the CMB results.

In the follow up paper Chisari et al. (2016) they try to constrain this anisotropic non-Gaussianity coefficient better by using multiple shear estimates like in the previous application description 3.2. This indeed improves the constrains on the anisotropic non-Gaussianity parameter.

In Schmidt et al. (2015) they show how implementing anisotropic non-Gaussianity in the galaxy shape correlation leads to a scale dependent bias in the shape. To be more precise, the linear alignment bias term b_I in the expression of γ (21) transforms in the presence of anisotropic non-Gaussianity as:

$$b_I \to b_I + 3b_I^{NG} A_2 M^{-1}(k, z) \tag{94}$$

b_I^{NG} is a bias that describes the response of the galaxy shape to an anisotropic initial power spectrum of small scale density perturbations. The assumption made in the paper is that b_I^{NG} is comparable to b_I as:

$$b_I^{NG} = \tilde{b}_I^{NG} b_I(z) \frac{D(z)}{D(0)} \tag{95}$$

And taking $\tilde{b}_I^{NG} = 1$, but keeping track of its real value by calculating the constraints of anisotropic non-Gaussianity parameter $A_2 \times \tilde{b}_I^{NG}$. The M term gives the relation between the overdensity δ and the primordial potential ψ

$$M(k, z) = \frac{2}{3} \frac{k^2 T(k) D(z)}{\Omega_m H_0^2} \tag{96}$$

$T(k)$ is the matter transfer function at $z = 0$. All the correlations which contain the shape of galaxies are then affected by the change of this linear alignment bias term when the non-Gaussianities are taken into account. This means that it is present in the galaxy-shape correlation but also in the velocity-shape correlation. The transformation of the linear alignment bias when non-Gaussianities are present can be implemented in the velocity shape correlation power spectrum (64) in the following way:

$$P_{v_r E}(k, \mu, z) = b_I b_v f a H (1 - \mu^2) \mu \frac{1}{k} P_{\delta\delta}(k, z) \tag{97}$$

$$P_{v_rE}(k, \mu, z) = [b_I + 3b_I^{NG} A_2 M^{-1}(k, z)] b_v f a H (1 - \mu^2) \mu \frac{1}{k} P_{\delta\delta}(k, z) \tag{98}$$

The same can be done for the galaxy-shape power spectrum:

$$P_{gE}(k, \mu, z) = [b_I + 3b_I^{NG} A_2 M^{-1}(k, z)](1 - \mu^2)(b_g + f\mu^2) P_{\delta\delta}(k, z) \tag{99}$$

To make a prediction of how adding velocity-shape correlation can improve on constraining the anisotropic non-Gaussianity parameter A_2, two Fisher forecasts are done. One that combines the information of P_{gE} and P_{v_rE} to constrain $A_2\tilde{b}_I^{NG}$ to see if this improves on the results from Schmidt et al. (2015). Another with the same combination of power spectra but with implementing multiple shear estimates. This is done by adding on top of P_{gE} and P_{v_rE} the same power spectra with different alignment amplitudes, like if they are measured with a different shear estimate. Comparing those results with the constraining values of A_2 in Chisari et al. (2016).

So first the Fisher forecast with a single shape measurement is done. Here combining P_{gE} and P_{v_rE} to calculate the Fisher value is done in the same way as (92) but now with respect to $A_2\tilde{b}_I^{NG}$. The following expression is calculated for LSST data:

$$F_{(A_2\tilde{b}_I^{NG})(A_2\tilde{b}_I^{NG})} = \frac{V_{survey}}{(2\pi)^2} \int_{k_{min}}^{k_{max}} dk \, k^2 \times$$

$$\left[\left(\frac{\partial P_{gE}^{(0)}(k)}{\partial(A_2\tilde{b}_I^{NG})} \right)^2 \frac{1}{\sigma^2_{P_{gE}^{(0)} P_{gE}^{(0)}}} + 2 \frac{\partial P_{gE}^{(0)}(k)}{\partial(A_2\tilde{b}_I^{NG})} \frac{1}{\sigma_{P_{gE}^{(0)} P_{v_rE}^{(1)}}} \frac{\partial P_{v_rE}^{(1)}(k)}{\partial(A_2\tilde{b}_I^{NG})} + \left(\frac{\partial P_{v_rE}^{(1)}(k)}{\partial(A_2\tilde{b}_I^{NG})} \right)^2 \frac{1}{\sigma^2_{P_{v_rE}^{(1)} P_{v_rE}^{(1)}}} \right] \tag{100}$$

In Schmidt et al. (2015) also a LSST like survey was used and the result from their Fisher forecast was a constraining of $\Delta(\tilde{b}_{NG}^I A_2) = 150$ using a multipole range of $2 \leq l \leq 600$. This was slightly less accurate than the measurements from the CMB: $\Delta A_2^{CMB} \sim 90$. The Fisher forecast as shown above leads to the result of $\Delta(\tilde{b}_{NG}^I A_2) = 988$.

Secondly the same Fisher forecast is done but with an extra set of power spectra with a difference in the alignment amplitude of 20%. The expression of the Fisher value is then the following:

$$F_{(A_2\tilde{b}_I^{NG})(A_2\tilde{b}_I^{NG})} = \frac{V_{survey}}{(2\pi)^2} \int_{k_{min}}^{k_{max}} dk \, k^2 \times \left[\left(\frac{\partial P_{gE}^{(0)}(k)}{\partial(A_2\tilde{b}_I^{NG})} \right)^2 \frac{1}{\sigma^2_{P_{gE}^{(0)} P_{gE}^{(0)}}} \right.$$

$$+ 2 \frac{\partial P_{gE}^{(0)}(k)}{\partial(A_2\tilde{b}_I^{NG})} \frac{1}{\sigma_{P_{gE}^{(0)} P_{v_rE}^{(1)}}} \frac{\partial P_{v_rE}^{(1)}(k)}{\partial(A_2\tilde{b}_I^{NG})} + \left(\frac{\partial P_{v_rE}^{(1)}(k)}{\partial(A_2\tilde{b}_I^{NG})} \right)^2 \frac{1}{\sigma^2_{P_{v_rE}^{(1)} P_{v_rE}^{(1)}}} + \left(\frac{\partial P_{gE,2}^{(0)}(k)}{\partial(A_2\tilde{b}_I^{NG})} \right)^2 \frac{1}{\sigma^2_{P_{gE,2}^{(0)} P_{gE,2}^{(0)}}}$$

$$\left. + 2 \frac{\partial P_{gE,2}^{(0)}(k)}{\partial(A_2\tilde{b}_I^{NG})} \frac{1}{\sigma_{P_{gE,2}^{(0)} P_{v_rE,2}^{(1)}}} \frac{\partial P_{v_rE,2}^{(1)}(k)}{\partial(A_2\tilde{b}_I^{NG})} + \left(\frac{\partial P_{v_rE,2}^{(1)}(k)}{\partial(A_2\tilde{b}_I^{NG})} \right)^2 \frac{1}{\sigma^2_{P_{v_rE,2}^{(1)} P_{v_rE,2}^{(1)}}} \right] \tag{101}$$

With the subscript 2 meaning the second set of power spectra with a different alignment amplitude. The result of this calculation can be compared with those from Chisari et al. (2016) for LSST data with only red galaxies and multi tracing with multiple shear measurements; $\Delta(\tilde{b}_I^{\mathrm{NG}} A_2) = 94$. Above calculation gives a result of $\Delta(\tilde{b}_{\mathrm{NG}}^I A_2) = 768$.

Both fractional errors are much bigger than the ones from the papers. However the comparison is not so straight forward to make. For example in the paper of Chisari et al. (2016) they looked at P_{gg}, P_{gE}, P_{EE} with different shape measurements on P_{gE}, P_{EE}. So they already took more information than in the Fisher forecast done here, where only P_{gE}, P_{vE} are taken into account with different shape measurements. That this gives lesser constraints is then quite expected.

4   Conclusion and discussion

To predict the measurability of the velocity-shape correlation a Fisher forecast was done based on the data of the upcoming survey LSST. The results are promising which is in line with the results from Okumura et al. (2019), Okumura et al. (2020) (see 2.4). The fractional error for the alignment strength is small which indicates that the alignment of galaxy shapes with the large scale velocity field should be visible in the data. Furthermore when comparing with the results from the galaxy density-shape correlations, a lower fractional error, around a factor of ten, for the alignment strength is found and also a somewhat lower signal to noise for the power spectrum signal. This alignment correlation is already measured for Luminous Red Galaxies as mentioned in section 2.1.4. The uncertainties for the velocity-shape correlations are thus a bit larger, seen from the larger signal to noise. But the signal to noise ratios are in the same ballpark indicating a good probability for also measuring velocity-shape correlation. Due to the larger uncertainties of the velocity-shape correlation the fractional error for the alignment strength is bigger. Still it is quite small, so a positive result.

However a few things are important to keep in mind. A Fisher forecast gives the best possible prediction of the outcome of the real measurement. So the details of the measurement determine of the real results will be comparable to this Fisher forecast. Furthermore the used values of, among other things, the mean redshift, red fraction and the number density are coming from the data for the upcoming LSST survey. LSST probes the sky to quite high redshift, $z \sim 1$. The higher the redshift the more lensing effects there are, because of more foreground galaxies in your survey. In addition is LSST a photometric survey with which it is harder to separate the weak lensing effects from the intrinsic alignment effects then with a spectroscopic survey. Therefore the same prediction was done for the spectroscopic 4MOST survey for which the IA effects can be separated from the lensing effects. This survey lies within LSST and has a lower galaxy number density and smaller volume. The fractional errors for the alignment strength are bigger than for the LSST survey and the signal to noise ratios for the power spectra. This was expected because of the smaller number density and volume. Still, the fractional errors are quite small and the signal to noise ratios sufficient. So also this measurement gives a positive results for the measurability of the velocity-shape correlation in the data.

For two of the discussed applications a rough estimate of the improvement of implementing velocity-shape correlation is done. For the application of determining the scale dependence of the alignment model with multiple shape measurements, a Fisher forecast up to linear order of the change in the alignment power spectra is done. This could say something about how well the improvement of implementing velocity-shape correlation is in constraining this change. The better this change can be constrained, the better the scale dependence of the model on small scales can be constructed with multiple shape measurements. The forecast predicted an improvement around an order of ten on the fractional error of the change. Keeping in mind that this calculation is just a first step in looking into how velocity-shape correlation can improve and only the change up to linear order is taken into account. These results shows that it is an interesting implementation and encourages further research on the topic.

The results of the estimation made for the improvement on implementing velocity-shape correlation to constrain the anisotropic non-Gaussianity parameter are less encouraging. The re-

sults from the Fisher forecast on implementing velocity-shape correlation to the non-Gaussian forecast and to the non-Gaussian forecast for multiple shape measurements are both quite off, compared to the results from the discussed papers (resp. Schmidt et al. 2015, Chisari et al. 2016). The fractional error for the anisotropic non-Gaussinity parameter from the first forecast is close to a factor ten higher and for the second one around a factor eight higher. Although this comparison was not that fair to make because of the different approach in the Fisher calculation (3.3). It is not an immediate invitation to look further into this implementation but it also should not be dismissed. With a more comparable approach the results are expected to be better.

There is no estimation done for the improvements for constraining the selection effects induced by alignments. However it is qualitatively promising. When putting forward the correlations that are affected by the selection affect, for example P_{gE}, and the correlations that up to linear order are not, for example P_{vE}, to compare the measurements of respectively (f+A) and f, one has to keep in mind that these correlations that are free of this effect are only up to linear order. This method would then expected to work on the large scales where the linear limit is applicable. This expectation can be supported by comparison of ξ_{g+} and ξ_{v+} in real and redshift space done in Okumura et al. (2020) also discussed in 2.4. Because the selection effects mimics the effect of redshift space distortions, looking at those results can say something about the selection effects as well. From their results it could be concluded that on large scales the difference for real and redshift space for P_{v+} are indeed negligible but not for P_{g+}. Similar results for the selection effects could be therefore expected as well. In the discussion of this application, three correlations that are influenced by the selection effect are summed up and three that are not, because those multiple correlations can be combined, the degeneracies in determining A can be lifted.

5   Outlook

The results from the predictions done for both surveys seem to indicate that the velocity-shape correlation will be measurable in the upcoming surveys. To be even more complete one should implement the weak lensing effects in the Fisher forecast for LSST to see how this changes the results.

Another improvement would be to refine the forecast. In this thesis the average redshift of LSST is taken and the according red fraction and linear alignment bias of this average redshift are used. It would be more accurate when taking the different values of the red fraction and alignment bias for the different redshifts into account.

After improving on this prediction and having stronger evidence of the measurability of the velocity-shape correlation, the next step would be to try and measure this correlation with the data from upcoming surveys as LSST. This would give more alignment data which leads to a higher constraining power for determining cosmological parameter. For example, from the results of Okumura et al. (2019) it can be expected that BAO information can be extracted from velocity-shape correlation as well as discussed in section 2.4.

The discussion of possible applications of the velocity-shape correlations in 3 can be improved as well. For the application of the selection effect induced by alignment one could also do a Fisher forecast to predict how good the selection parameter 'A' can be constraint. If this gives promising results the next step would be to measure f and (f+A) from the data with the proposed correlations 3.1.

The Fisher forecast done for predicting the effect of implementing velocity-shape correlation to the multiple shape measurements, is only a rough estimate. This could be refined by looking at the change due to using different shape measurements up to higher order and with a change parameter that is not necessarily a constant. However from the method in this thesis it already showed some promising results, so if this also shows up in the more refined estimates, the next step would be to actually implement the velocity-shape correlation to better constrain the scale dependence of the model on small scales.

The Fisher forecast done for the anisotropic non-Gaussianity parameter is not very encouraging for further implementation. However when following a forecast that is more comparable to what is done in the papers (Schmidt et al. 2015, Chisari et al. 2016), the results may be more significant.

Acknowledgements

This thesis would not have been possible without all the help from my supervisor Dr. N.E. Chisari. I would like to thank her for all the time she took out for our weekly meetings with valuable feedback, the many articles she recommended and the checks on calculations, code and text. It was really helpful that she always was willing to answer questions and that she facilitated the group meetings. In addition I would like to mention all the help from C. Vedder, R. Nederstigt and W. Doumerg during the group meetings and after. Last, I want to thank T. van Gemeren, M. Zijderveld and N. Boertjes for reading this thesis and for their feedback.

References

J. Blazek, M. McQuinn, and U. Seljak. Testing the tidal alignment model of galaxy intrinsic alignment. , 2011(5):010, May 2011. doi: 10.1088/1475-7516/2011/05/010.

S. Bridle and L. King. Dark energy constraints from cosmic shear power spectra: impact of intrinsic alignments on photometric redshift requirements. *New Journal of Physics*, 9(12): 444, Dec. 2007. doi: 10.1088/1367-2630/9/12/444.

M. L. Brown, A. N. Taylor, N. C. Hambly, and S. Dye. Measurement of intrinsic alignments in galaxy ellipticities. , 333(3):501–509, July 2002. doi: 10.1046/j.1365-8711.2002.05354.x.

P. Catelan, M. Kamionkowski, and R. D. Blandford. Intrinsic and extrinsic galaxy alignment. , 320(1):L7–L13, Jan. 2001. doi: 10.1046/j.1365-8711.2001.04105.x.

N. E. Chisari and C. Dvorkin. Cosmological information in the intrinsic alignments of luminous red galaxies. , 2013(12):029, Dec. 2013. doi: 10.1088/1475-7516/2013/12/029.

N. E. Chisari, C. Dvorkin, F. Schmidt, and D. N. Spergel. Multitracing anisotropic non-Gaussianity with galaxy shapes. , 94(12):123507, Dec. 2016. doi: 10.1103/PhysRevD.94. 123507.

N. E. Chisari, D. Alonso, E. Krause, C. D. Leonard, P. Bull, J. Neveu, A. Villarreal, S. Singh, T. McClintock, J. Ellison, Z. Du, J. Zuntz, A. e. Mead, S. Joudaki, C. S. Lorenz, T. Tröster, J. Sanchez, F. Lanusse, M. Ishak, R. Hlozek, J. Blazek, J.-E. Campagne, H. Almoubayyed, T. Eifler, M. Kirby, D. Kirkby, S. Plaszczynski, A. Slosar, M. Vrastil, E. L. Wagoner, and LSST Dark Energy Science Collaboration. Core Cosmology Library: Precision Cosmological Predictions for LSST. , 242(1):2, May 2019. doi: 10.3847/1538-4365/ab1658.

D. Clowe, M. Bradač, A. H. Gonzalez, M. Markevitch, S. W. Randall, C. Jones, and D. Zaritsky. A Direct Empirical Proof of the Existence of Dark Matter. , 648(2):L109–L113, Sept. 2006. doi: 10.1086/508162.

DESI Collaboration et al. The DESI Experiment Part I: Science,Targeting, and Survey Design. *arXiv e-prints*, art. arXiv:1611.00036, Oct. 2016.

S. Dodelson. *Modern cosmology*. Academic Press, 1 edition, 2003.

C. A. J. Duncan, B. Joachimi, A. F. Heavens, C. Heymans, and H. Hildebrandt. On the complementarity of galaxy clustering with cosmic shear and flux magnification. , 437(3): 2471–2487, Jan. 2014. doi: 10.1093/mnras/stt2060.

A. Friedmann. Über die Krümmung des Raumes. *Zeitschrift fur Physik*, 10:377–386, Jan. 1922. doi: 10.1007/BF01332580.

A. H. Guth. Inflationary universe: A possible solution to the horizon and flatness problems. , 23(2):347–356, Jan. 1981. doi: 10.1103/PhysRevD.23.347.

C. M. Hirata. Tidal alignments as a contaminant of redshift space distortions. , 399(2): 1074–1087, Oct. 2009. doi: 10.1111/j.1365-2966.2009.15353.x.

C. M. Hirata, R. Mandelbaum, M. Ishak, U. Seljak, R. Nichol, K. A. Pimbblet, N. P. Ross, and D. Wake. Intrinsic galaxy alignments from the 2SLAQ and SDSS surveys: luminosity and redshift scalings and implications for weak lensing surveys. , 381(3):1197–1218, Nov. 2007. doi: 10.1111/j.1365-2966.2007.12312.x.

E. Hubble. A Relation between Distance and Radial Velocity among Extra-Galactic Nebulae. *Proceedings of the National Academy of Science*, 15(3):168–173, Mar. 1929. doi: 10.1073/pnas.15.3.168.

Ž. Ivezić et al. LSST: From Science Drivers to Reference Design and Anticipated Data Products. , 873(2):111, Mar. 2019. doi: 10.3847/1538-4357/ab042c.

B. Joachimi, R. Mandelbaum, F. B. Abdalla, and S. L. Bridle. Constraints on intrinsic alignment contamination of weak lensing surveys using the MegaZ-LRG sample. , 527: A26, Mar. 2011. doi: 10.1051/0004-6361/201015621.

H. Johnston, C. Georgiou, B. Joachimi, H. Hoekstra, N. E. Chisari, D. Farrow, M. C. Fortuna, C. Heymans, S. Joudaki, K. Kuijken, and A. Wright. KiDS+GAMA: Intrinsic alignment model constraints for current and future weak lensing cosmology. , 624:A30, Apr. 2019. doi: 10.1051/0004-6361/201834714.

N. Kaiser. Clustering in real space and in redshift space. , 227:1–21, July 1987. doi: 10.1093/mnras/227.1.1.

T. Kurita, M. Takada, T. Nishimichi, R. Takahashi, K. Osato, and Y. Kobayashi. Power spectrum of halo intrinsic alignments in simulations. *arXiv e-prints*, art. arXiv:2004.12579, Apr. 2020.

C. D. Leonard, R. Mandelbaum, and LSST Dark Energy Science Collaboration. Measuring the scale dependence of intrinsic alignments usingmultiple shear estimates. , 479(1):1412–1426, Sept. 2018. doi: 10.1093/mnras/sty1444.

A. Lewis and A. Challinor. CAMB: Code for Anisotropies in the Microwave Background, Feb. 2011.

R. Mandelbaum, C. M. Hirata, M. Ishak, U. Seljak, and J. Brinkmann. Detection of large-scale intrinsic ellipticity-density correlation from the Sloan Digital Sky Survey and implications for weak lensing surveys. , 367(2):611–626, Apr. 2006. doi: 10.1111/j.1365-2966.2005.09946.x.

R. Mandelbaum, C. Blake, S. Bridle, F. B. Abdalla, S. Brough, M. Colless, W. Couch, S. Croom, T. Davis, M. J. Drinkwater, K. Forster, K. Glazebrook, B. Jelliffe, R. J. Jurek, I. H. Li, B. Madore, C. Martin, K. Pimbblet, G. B. Poole, M. Pracy, R. Sharp, E. Wisnioski, D. Woods, and T. Wyder. The WiggleZ Dark Energy Survey: direct constraints on blue galaxy intrinsic alignments at intermediate redshifts. , 410(2):844–859, Jan. 2011. doi: 10.1111/j.1365-2966.2010.17485.x.

D. Martens, C. M. Hirata, A. J. Ross, and X. Fang. A radial measurement of the galaxy tidal alignment magnitude with BOSS data. , 478(1):711–732, July 2018. doi: 10.1093/mnras/sty1100.

T. Okumura and A. Taruya. Anisotropies of galaxy ellipticity correlations in real and redshift space: angular dependence in linear tidal alignment model. , 493(1):L124–L128, Mar. 2020. doi: 10.1093/mnrasl/slaa024.

T. Okumura, A. Taruya, and T. Nishimichi. Intrinsic alignment statistics of density and velocity fields at large scales: Formulation, modeling, and baryon acoustic oscillation features. , 100(10):103507, Nov. 2019. doi: 10.1103/PhysRevD.100.103507.

T. Okumura, A. Taruya, and T. Nishimichi. Testing tidal alignment models for anisotropic correlations of halo ellipticities with N-body simulations. , 494(1):694–702, Mar. 2020. doi: 10.1093/mnras/staa718.

S. Perlmutter, G. Aldering, G. Goldhaber, R. A. Knop, P. Nugent, P. G. Castro, S. Deustua, S. Fabbro, A. Goobar, D. E. Groom, I. M. Hook, A. G. Kim, M. Y. Kim, J. C. Lee, N. J. Nunes, R. Pain, C. R. Pennypacker, R. Quimby, C. Lidman, R. S. Ellis, M. Irwin, R. G. McMahon, P. Ruiz-Lapuente, N. Walton, B. Schaefer, B. J. Boyle, A. V. Filippenko, T. Matheson, A. S. Fruchter, N. Panagia, H. J. M. Newberg, W. J. Couch, and T. S. C. Project. Measurements of Ω and Λ from 42 High-Redshift Supernovae. , 517(2):565–586, June 1999. doi: 10.1086/307221.

Planck Collaboration et al. Planck 2018 results. VI. Cosmological parameters. *arXiv e-prints*, art. arXiv:1807.06209, July 2018.

J. Richard, J. P. Kneib, C. Blake, A. Raichoor, J. Comparat, T. Shanks, J. Sorce, M. Sahlén, C. Howlett, E. Tempel, R. McMahon, M. Bilicki, B. Roukema, J. Loveday, D. Pryer, T. Buchert, C. Zhao, and CRS Team. 4MOST Consortium Survey 8: Cosmology Redshift Survey (CRS). *The Messenger*, 175:50–53, Mar. 2019. doi: 10.18727/0722-6691/5127.

A. G. Riess, A. V. Filippenko, P. Challis, A. Clocchiatti, A. Diercks, P. M. Garnavich, R. L. Gilliland, C. J. Hogan, S. Jha, R. P. Kirshner, B. Leibundgut, M. M. Phillips, D. Reiss, B. P. Schmidt, R. A. Schommer, R. C. Smith, J. Spyromilio, C. Stubbs, N. B. Suntzeff, and J. Tonry. Observational Evidence from Supernovae for an Accelerating Universe and a Cosmological Constant. , 116(3):1009–1038, Sept. 1998. doi: 10.1086/300499.

B. Ryden. *Introduction to cosmology*. Cambridge University Press, 2 edition, 2017.

S. Samuroff, J. Blazek, M. A. Troxel, N. MacCrann, E. Krause, C. D. Leonard, J. Prat, D. Gruen, S. Dodelson, T. F. Eifler, M. Gatti, W. G. Hartley, B. Hoyle, P. Larsen, J. Zuntz, T. M. C. Abbott, S. Allam, J. Annis, G. M. Bernstein, E. Bertin, S. L. Bridle, D. Brooks, A. Carnero Rosell, M. Carrasco Kind, J. Carretero, F. J. Castander, C. E. Cunha, L. N. da Costa, C. Davis, J. De Vicente, D. L. DePoy, S. Desai, H. T. Diehl, J. P. Dietrich, P. Doel, B. Flaugher, P. Fosalba, J. Frieman, J. García-Bellido, E. Gaztanaga, D. W. Gerdes, R. A. Gruendl, J. Gschwend, G. Gutierrez, D. L. Hollowood, K. Honscheid, D. J. James, K. Kuehn, N. Kuropatkin, M. Lima, M. A. G. Maia, M. March, J. L. Marshall,

P. Martini, P. Melchior, F. Menanteau, C. J. Miller, R. Miquel, R. L. C. Ogando, A. A. Plazas, E. Sanchez, V. Scarpine, R. Schindler, M. Schubnell, S. Serrano, I. Sevilla-Noarbe, E. Sheldon, M. Smith, F. Sobreira, E. Suchyta, G. Tarle, D. Thomas, V. Vikram, and DES Collaboration. Dark Energy Survey Year 1 results: constraints on intrinsic alignments and their colour dependence from galaxy clustering and weak lensing. , 489(4):5453–5482, Nov. 2019. doi: 10.1093/mnras/stz2197.

F. Schmidt, N. E. Chisari, and C. Dvorkin. Imprint of inflation on galaxy shape correlations. , 2015(10):032, Oct. 2015. doi: 10.1088/1475-7516/2015/10/032.

M. D. Schneider and S. Bridle. A halo model for intrinsic alignments of galaxy ellipticities. , 402(4):2127–2139, Mar. 2010. doi: 10.1111/j.1365-2966.2009.15956.x.

Simons Observatory Collaboration et al. The Simons Observatory: science goals and forecasts. , 2019(2):056, Feb. 2019. doi: 10.1088/1475-7516/2019/02/056.

S. Singh and R. Mandelbaum. Intrinsic alignments of BOSS LOWZ galaxies - II. Impact of shape measurement methods. , 457(3):2301–2317, Apr. 2016. doi: 10.1093/mnras/stw144.

S. Singh, R. Mandelbaum, and S. More. Intrinsic alignments of sdss-iii boss lowz sample galaxies. *Monthly Notices of the Royal Astronomical Society*, 450(2):2195–2216, 06 2015. doi: 10.1093/mnras/stv778.

K. M. Smith, M. S. Madhavacheril, M. Münchmeyer, S. Ferraro, U. Giri, and M. C. Johnson. ksz tomography and the bispectrum. 10 2018.

M. A. Strauss, D. H. Weinberg, R. H. Lupton, V. K. Narayanan, J. Annis, M. Bernardi, M. Blanton, S. Burles, A. J. Connolly, J. Dalcanton, M. Doi, D. Eisenstein, J. A. Frieman, M. Fukugita, J. E. Gunn, Ž. Ivezić, S. Kent, R. S. J. Kim, G. R. Knapp, R. G. Kron, J. A. Munn, H. J. Newberg, R. C. Nichol, S. Okamura, T. R. Quinn, M. W. Richmond, D. J. Schlegel, K. Shimasaku, M. SubbaRao, A. S. Szalay, D. Vanden Berk, M. S. Vogeley, B. Yanny, N. Yasuda, D. G. York, and I. Zehavi. Spectroscopic Target Selection in the Sloan Digital Sky Survey: The Main Galaxy Sample. , 124(3):1810–1824, Sept. 2002. doi: 10.1086/342343.

A. Taruya and T. Okumura. Improving Geometric and Dynamical Constraints on Cosmology with Intrinsic Alignments of Galaxies. , 891(2):L42, Mar. 2020. doi: 10.3847/2041-8213/ab7934.

D. H. Weinberg, M. J. Mortonson, D. J. Eisenstein, C. Hirata, A. G. Riess, and E. Rozo. Observational probes of cosmic acceleration. , 530(2):87–255, Sept. 2013. doi: 10.1016/j.physrep.2013.05.001.

H.-M. Zhu, M. White, S. Ferraro, and E. Schaan. Reconstruction with velocities. Apr. 2020.

A Appendix

A.1 Core cosmology library

The power spectra and other related functions and parameters for the various Fisher forecasts that are done in this thesis, are calculated with the latest version (v2.1.0) of the Python package 'Core cosmology library (CCL)'. The library is mostly developed for making cosmological predictions for analysing the data from the upcoming LSST survey and it is available at https://github.com/LSSTDESC/CCL. A very elaborate description of the quantities that are provided by the library is given by Chisari et al. (2019). In this Appendix section a clarification is given about what cosmological quantities for the executed forecasts are calculated with CCL.

Before any predictions can be calculated with CCL, one must define the used cosmology in terms of the value for the density parameter of cold dark matter and baryons at $z = 0$, the reduced Hubble constant, the amplitude and power of the primordial power spectrum. The cosmology used for the calculations in this thesis is:

$$cosmo = ccl.Cosmology(Omegac = 0.27, Omegab = 0.045, h = 0.67, As = 2.1e^{-9}, ns = 0.96)$$

Hereafter the specification of the needed parameters for the forecast was done. Cosmological parameters as the growth rate f, the Hubble parameter H, and the growth factor D can be calculated by the library as functions of the defined cosmology and scale factor a. Then one can start calculating the required power spectra. The matter power spectrum is a standard function in CCL as a function of the cosmology, k and a. It provides both the linear and non-linear matter power spectrum. By adding the other required cosmological parameters one can build up the specific power spectrum from the matter power spectrum. The power spectrum can be used as a function, it can be plotted and integrated.

In the forecast where the non-Gaussianities are implemented (see 3.3) the transfer function needed to be calculated. For this, besides CCL also CAMB (Code for Anisotropies in the Microwave Background) should be installed (Lewis and Challinor 2011). CAMB provides the data for the transfer function with respect to the used cosmology. This can be combined with functions from CCL. One note to make is that CAMB gives the transfer function data as a number float, which can be plotted but it is not a function. When one wants to combine it with other functions or integrate over the transfer function, an interpolation of the data is required to get a function through the transfer function data.

A.2 LSST

The forecast for the velocity-shape correlation is based on the data for the upcoming LSST survey as described in Ivezić et al. (2019). In this Appendix section therefore a little bit of background information about this survey based on https://www.lsst.org/. The Vera C. Rubin Observatory, which was previously called the Large Synoptic Survey Telescope (LSST) is a large observatory located in Chile. The main survey will be the Legacy Survey of Space and Time (LSST) and will start operating in 2023. This survey will collect data for 10 years. The 8.4 meter Simonyi Survey Telescope has a wide view of 9.6 square degrees. In total LSST will cover 18 000 square degrees with around 800 visits of each spot creating a video

like recording of space. The for cosmology most important goals are the measurements of weak lensing, BAOs and type Ia supernovae as functions of the redshift.